SPECTROSCOPY AND PHOTOCHEMISTRY OF POLYATOMIC ALKALINE EARTH CONTAINING MOLECULES

Peter F. Bernath
Department of Chemistry, University of Waterloo, Waterloo, Ontario, Canada N2L 3G1

CONTENTS

Advances in Photochemistry, Volume 23. Edited by Douglas C. Neckers, David H. Volman, and Günther von Bünau
ISBN 0-471-19289-9

I. INTRODUCTION

The interaction of metals with organic molecules is one of the primary themes of modern chemistry [1]. This interest is based both on the possibility of important applications and on the fascinating variety of molecules that can be synthesized. Synthetic chemists working at the interface between organic and inorganic chemistry create new species and characterize them primarily by nuclear magnetic resonance (NMR) and X-ray crystallography. Many of their creations have found great utility in, for example, the Ziegler–Natta polymerization of ethylene to make polyethylene [1]. Metal–ligand interactions are also important in the chemistry of life processes at, for example, the active sites of enzymes. This new field of bioinorganic chemistry continues to expand.

All of this chemistry occurs in either solution or the solid state and is often influenced by the presence of a solvent. Currently, the tools of modern chemical physics are used to try to understand metal–ligand chemistry in the gas phase, free from the effects of solvents. The focus has been on understanding the chemistry, photochemistry, and spectroscopy of relatively small systems. For reasons of sensitivity, the primary tool for these investigations is the mass spectrometer. Sometimes lasers are used to vaporize a metal or to excite and to ionize the species of interest. The experimental techniques range from traditional high-pressure mass spectrometry to Fourier transform ion cyclotron resonance.

The photochemistry and spectroscopy of simple metal–ligand ions has been studied, for example, by the Brucat, Duncan, and Farrar research

groups. In the work of Lessen et al. [2], the vanadium ion (V^+) was created by laser vaporization and allowed to react with H_2O. The photodissociation of $V^+(H_2O)$ was driven by a tunable dye laser. The spectra were recorded by monitoring the appearance of V^+ with a time-of-flight (TOF) mass spectrometer as the laser was scanned. Similar work in the Duncan group has provided spectra of $Mg^+(H_2O)$ [3] and $Ca^+(H_2O)$ [4], while the Farrar group has looked at $Sr^+(H_2O)$ and $Sr^+(NH_3)$ [5,6]. These molecular ions are isoelectronic with the neutral molecules such as $CaNH_2$ and $SrCH_3$ that are discussed in this chapter.

Molecular ions such as $Ca^+(H_2O)$ have relatively weak metal–ligand binding energies of about 25 kcal mol^{-1} [7] compared to the stronger bond present in the isoelectronic $CaNH_2$ system. In $Ca^+(H_2O)$, the H_2O ligand perturbs the Ca^+ energy levels much less than the NH_2^- ligand perturbs Ca^+ in the $CaNH_2$ molecule. The electrostatic interaction of NH_2^- with Ca^+ is much stronger than the ion–dipole interaction of Ca^+ with H_2O, although the molecular symmetry (C_{2v}) is the same for $CaNH_2$ and $Ca^+(OH_2)$.

This chapter will cover the monovalent neutral polyatomic derivatives of the alkaline earth elements: Be, Mg, Ca, Sr, Ba, and Ra. The alkaline earth metals are naturally divalent in the solid state. Well-known examples of alkaline earth compounds are the widely used Grignard reagents, which have an empirical formula R—Mg—X (R is an alkyl group and X is a halogen) [1]. More recently, the Hanusa group at Vanderbilt has explored the organometallic chemistry of divalent Ca, Sr, and Ba derivatives [8]. In contrast to this "normal" chemistry, the monovalent derivatives such as CaOH are unstable in the solid state because they readily disproportionate:

$$2\,CaOH(s) \rightarrow Ca(s) + Ca(OH)_2(s) \qquad (1)$$

In fact, "proof" of the nonexistence of MgCl(s) is discussed in undergraduate chemistry textbooks as an exercise in calculating lattice energies using Madelung constants.

The monovalent derivatives of the alkaline earth metals are free radicals that are stable in the thermodynamic sense in the gas phase or when isolated in inert matrices. Molecules such as CaOH have strong bonds (dissociation energy, $D_{Ca-O} = 92$ kcal mol^{-1}) [9,10] but are very reactive species because of the unpaired electron localized on the Ca atom. In spite of the transient nature of these monovalent derivatives, it has proved possible to develop an extensive gas-phase inorganic chemistry for Mg, Ca, Sr, and Ba. No monovalent polyatomic derivatives are known for the Be or the Ra members of the alkaline earth group, except for BeOH. There are two experimental reports on the BeOH [11,12] molecule in

the literature but one is apparently erroneous [12]. For technical reasons, the widest variety of molecules are known for Ca and Sr.

In addition to the usual divalent molecules and solids, for example, $Ca(OH)_2$, and the monovalent molecules, for example, CaOH, a third type of molecule has been predicted by Kong and Boyd [13]. They calculate that the H—Ca—O isomer of CaOH is a minimum on the potential energy surface. The H—Ca—O molecule is, in fact, a divalent derivative of Ca with an ionic electron distribution, $H^-Ca^{2+}O^-$. Perhaps the ultraviolet (UV) photochemical isomerization of CaOH in a rare gas matrix will yield HCaO.

The metal monohydroxides CaOH and SrOH are the simplest monovalent polyatomic derivatives of the alkaline earths. Both CaOH and SrOH have a surprisingly long history in view of their high chemical reactivity. While CaOH and SrOH can only be stored when isolated in rare gas matrices [14], substantial steady-state concentrations exist in a variety of energetic environments.

In 1823, Herschel [15] in the *Transactions of the Royal Society of Edinburgh* published his observations of the colors of flames produced by the introduction of alkaline earth salts. The green color obtained with barium salts is due to BaOH and the reddish color characteristic of strontium salts is caused by SrOH. The red colors of fireworks can also be attributed to emission from SrOH [16]. It was not until the 1950s that modern flame studies [17, 18] identified the molecules that are responsible for the alkaline earth flame colors. In contrast to the alkaline earths, the flame colors of the alkali elements are produced by atomic emission. The formation of molecules such as CaOH and SrOH, in fact, greatly complicates the use of flame absorption and emission for the determination of the concentrations of alkaline earth elements in analytical chemistry.

The CaOH molecule is also predicted to be of importance in atmospheric chemistry and in astronomy. It has been speculated that the ablation of metals from meteors results in the formation of CaOH [19]. In chemical equilibrium calculations, Tsuji [20] predicted that CaOH should form in the atmospheres of cool oxygen-rich stars. Pesch [21] identified the CaOH molecule through absorption of the $\tilde{B}^2\Sigma^+ - \tilde{X}^2\Sigma^+$ transition near 550 nm. Pettersen and Hawley [22] confirmed this identification using the $\tilde{A}^2\Pi - \tilde{X}^2\Sigma^+$ bands near 620 nm. The recent availability of microwave and millimeter wave spectra of MgOH [23] and CaOH [24] have resulted in unsuccessful searches by radioastronomers. While the high-temperature environment of a stellar atmosphere encourages the formation of CaOH, the molecule does not readily form in cold interstellar clouds.

Interstellar molecular clouds are the sites of star formation and so are of great astronomical interest. In general, metal-containing molecules are not very abundant in dark molecular clouds because they are depleted onto grains. It was, therefore, with some surprise that the MgNC molecule [25, 26] and its isomer MgCN [27] were identified by radioastronomers in the circumstellar envelope of a carbon star. This finding has inspired the Ziurys [27] group to record the laboratory millimeter wave spectra of a large number of simple derivatives of Mg and Ca such as MgCCH and $CaCH_3$.

A review on the calcium- and strontium-containing polyatomic free radicals appeared in 1991 [28], but there has been significant progress since then. In addition to the radio astronomical and laboratory measurements of pure rotation spectra already mentioned, modern molecular beam technology has been used extensively in recent years. Molecular beam spectroscopy has led to an improved understanding of the electronic and vibronic structure of the larger free radicals such as CaC_5H_5 and CaC_4H_4N. It is time to cover the field again with a comprehensive review, emphazing the recent advances.

II. EXPERIMENTAL METHODS

A. Flames

The alkaline earth hydroxide molecules were first made in flames and studied by emission spectroscopy [15]. Metal salt solutions are aspirated into atmospheric pressure flames or the salts are placed on a loop of wire in the flame. The MOH (M is an alkaline earth metal) molecules form through a complicated set of flame reactions [18]. More recent flame work has included laser-induced fluorescence studies of CaOH [29] and SrOH [30]. Some of this work is motivated by the observation that soot formation is suppressed in flames when alkaline earths salts are added [31].

Although flames are convenient sources of MOH molecules, they suffer from serious drawbacks for spectroscopic and dynamical studies. The high temperature ($\sim$2000 K) of flames causes numerous vibrational and rotational levels to be populated resulting in very dense spectra. The high pressure (1 atm) broadens the rotational lines ($>0.1\ cm^{-1}$) and increases the overlap of the lines. In addition, resonant laser-induced fluorescence is difficult to detect because of quenching and the overwhelming presence of nonresonant fluorescence caused by rapid collisional energy transfer. The luminescence of the flame itself also interferes with measurements.

B. Broida Oven

The key discovery that opened up the field was made by Harris and co-workers [32–35] in the early 1980s. They found that alkaline earth monohydroxides and monoamides could be made readily in a flow reactor called a Broida oven [36]. The Broida oven is a relatively cool (~ 500 K), low-pressure (~ 5 torr) source of high-temperature molecules that is suitable for spectroscopic studies. The work of Harris and our own work owes a great debt to the pioneering efforts of Broida in developing the source and demonstrating its potential.

The Broida oven is a remarkable source of molecules. It offers a large concentration of free radicals ($\sim 10^{13}$ molecules cm^{-3}) isolated in a flow of inert carrier gas such as argon. In contrast to a molecular beam, a Broida oven also offers a large flux of molecules ($\sim 1\ g\ h^{-1}$) that could be used for preparative chemistry, although this aspect of the technology has never been exploited. The continuous injection of a room temperature carrier gas is responsible for both the large flux and the relatively low temperature of the source. Molecules produced in a furnace are sometimes called high-temperature molecules and the Broida oven offers the possibility of studying them near room temperature.

The molecular species in a Broida oven can often be detected through their chemiluminescent emission [32]. It is particularly convenient to monitor this emission in the early stages of a low-resolution analysis. The information that can be extracted from a chemiluminescent spectrum recorded with a monochromator is, however, limited. More typically, the molecules are detected by laser-induced fluorescence using either pulsed or continuous wave (CW) dye lasers.

The molecules in a Broida oven are produced by the reaction of a metal vapor with an appropriate oxidant (Fig. 1). The metal (Mg, Ca, Sr, or Ba) is vaporized in a resistively heated crucible and entrained in a flow of Ar gas. The oxidant is added at the top through an oxidant ring. The reaction of the metal with an oxidizer, for example,

$$Ca + H_2O \rightarrow CaOH + H \qquad (2)$$

often produces a low-pressure chemiluminescent flame above the oxidant injection ring (Fig. 1). The mechanism for this chemical reaction (2) is discussed below. Typical pressures are 5 torr of Ar carrier gas, 1 mtorr of metal vapor (Ca), and 10 mtorr of oxidant (H_2O). The resulting product (CaOH) has a concentration of less than 1 mtorr, perhaps as high as 10^{13} molecules cm^{-3} in the most favorable cases.

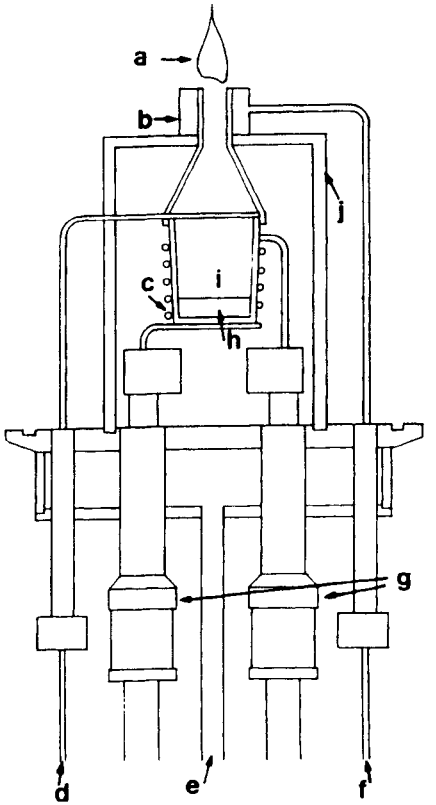

Figure 1. The baseplate for the Broida oven metal flow reactor. This baseplate is attached to the bottom of a vacuum chamber (Fig. 2). (a) chemiluminescent flame; (b) oxidant injection ring; (c) tungsten wire heating basket; (d) Ar carrier gas inlet; (e) cooling water; (f) oxidant gas inlet; (g) electrical feeds for heating; (h) alkaline earth metal; (i) alumina crucible; and (j) alumina heat shield. [Reprinted with permission from ref. 28. Copyright 1991 American Association for the Advancement of Science.]

During the course of our investigations, we found that if the metal atoms are excited by a laser to the metastable $^3P_1$ electronic state, then the concentration of product molecules is dramatically increased,

$$Ca^*(^3P_1) + H_2O \rightarrow CaOH + H, \qquad (3)$$

where the asterisk denotes electronic excitation. Reaction 2 is endothermic

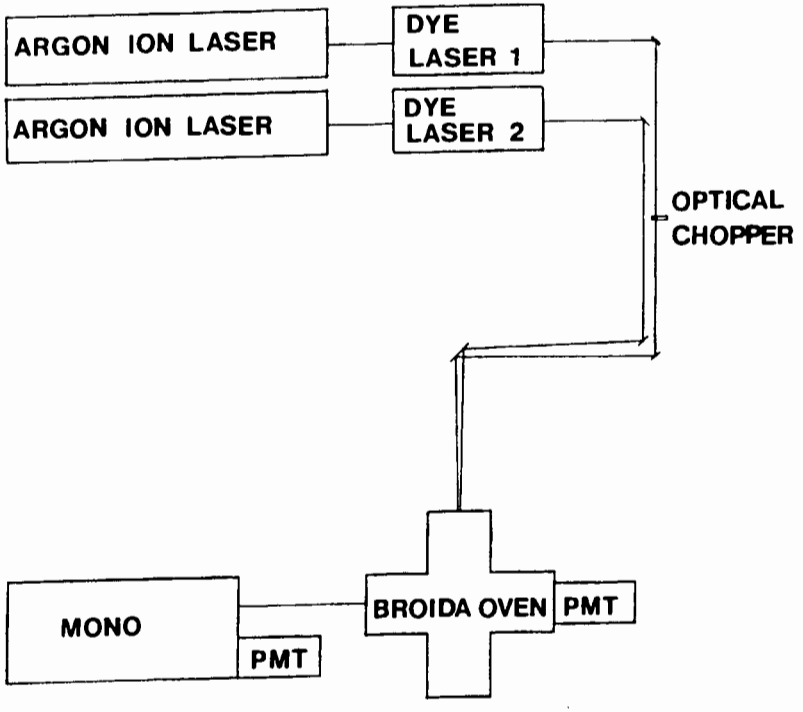

Figure 2. Experimental block diagram for Broida oven experiments in the Bernath laboratory. Two Ar ion lasers pump dye lasers that are used to make and to detect the free radicals in the oven. The laser-induced fluorescence is monitored with photomultiplier tubes (PMTs) mounted either directly on the oven or on the exit port of a monochromator (MONO). [Reprinted with permission from ref. 28. Copyright 1991 American Association for the Advancement of Science.]

as written but Reaction 3 can occur directly because the additional energy stored in Ca* makes Reaction 3 exothermic. The use of excited Ca atoms is particularly important for the formation of organometallic molecules such as CaC_5H_5 since ground-state Ca atoms will not react with the C_5H_6 precursor. Almost all of the molecules discussed in this chapter are produced through photochemistry.

Exploiting the enhanced reactivity of Ca* often requires the use of two tunable dye lasers (Fig. 2), one to excite the metal atoms to the metastable $^3P_1$ state and the second to detect the product molecules. (Excited metal atoms can also be produced in an electrical discharge or in a laser-vaporized plume.) The two laser beams are introduced into the Broida oven chamber

through Brewster angle windows on the top or the side. The first laser (dye laser 1) is tuned to the $^3P_1 - {}^1S_0$ atomic transition at 457.1, 657.3, 689.2 and, 791.1 nm for Mg, Ca, Sr, and Ba, respectively. This first laser is a typically operated broadband ($\sim$1- cm^{-1} line width) although an étalon is sometimes used to increase the spectral power density and the stability. The second laser (dye laser 2) can be operated broadband for survey work or in single longitudinal mode ($\sim$1-MHz bandwidth) for high-resolution work. In our laboratory, the lasers we use are the Coherent model 599, 699–29, and 899–29 dye lasers and a titanium sapphire laser, all pumped by Ar ion lasers. The typical laser powers are 0.5 W at the Broida oven. The two dye laser beams are spatially overlapped and focused into the Broida oven.

The first laser beam can be amplitude modulated ($\sim$1 kHz) with an optical chopper (Fig. 2), which modulates the concentration of the excited metal atoms, M*. Because the excited metal atoms have a much higher reactivity, the concentration of product molecules is also modulated. The modulated fluorescence excited by the second laser is then detected by a PMT and a lock-in amplifier. A monochromator or an optical filter is used to analyze the emission and to control the optical bandwidth detected by the PMT. This photochemical modulation and synchronous detection of the fluorescent signal is a very powerful technique for increasing the signal-to-noise (S/N) ratio.

There are two typical spectroscopic experiments. In the first, both lasers are in resonance with atomic (laser 1) and molecular (laser 2) transitions and the monochromator (Fig. 2) is scanned to record the laser-induced fluorescence. In the second type of experiment, the monochromator is used as a filter and is not scanned while the second laser wavelength is changed. This second type of experiment is called a laser excitation scan since a fluorescent signal is detected by the PMT only when laser 2 is in resonance with a molecular transition. In this case, the scanning laser can be broadband for survey work or single mode for high-resolution experiments.

The high-resolution spectra recorded with a Broida oven are limited by the effects of Doppler and collisional broadening. For example, in the visible region with a pressure of 10 torr, Doppler broadening dominates and a typical line width for a molecule like CaCCH is about 0.03 cm^{-1}. Nonlinear techniques such as intermodulated fluorescence are feasible in a Broida oven in order to remove the effects of Doppler broadening. The technique of laser excitation spectroscopy with selective fluorescence detection is often necessary to simplify the complex rotational structure of a molecule such as $CaCH_3$. Ultimately, the collisional redistribution of the excited state population in a Broida oven limits the size of molecule for which a rotational analysis is possible. For example, the rovibronic lines of CaC_5H_5 cannot be resolved in a Broida oven and a molecular beam experiment is necessary.

One of the recent developments has been the use of Broida oven technology in recording millimeter wave pure rotational spectra (Fig. 3). The pure rotational transitions are recorded in absorption using a free space cell. There are two main groups working in this area, the Ziurys group at Arizona State University [37] and the Saito group [25] at the Institute for Molecular Science in Japan.

In the Arizona State University design, the radiation is collimated with Teflon lenses and passes twice through the Broida oven. This double passing is achieved (Fig. 3) by sending the radiation through a wire grid polarizer, then reflecting the radiation with a rooftop prism oriented in such a way to rotate the plane of linear polarization by 90°. The return beam through the cell is now totally reflected by the polarizer and focused onto an InSb hot electron bolometer detector.

The source of microwave radiation at Arizona State University is a set of three phase-locked Gunn oscillators (Fig. 3), which operate in the 65–140-GHz region at power levels of about 50 mW. Higher frequencies are obtained by doubling, tripling, or quadrupling the fundamental frequency in a nonlinear Schottky diode multiplier. The millimeter wave radiation is frequency modulated at 25 kHz by adjusting the reference frequency used in the lock circuit.

The main difficulty in adapting the Broida oven to "low"-frequency millimeter wave measurements is the problem of pressure broadening [38]. Since the Doppler broadening of molecular lines is linearly proportional to the transition frequency, the Doppler effect is negligible in the millimeter wave region. The molecular line widths are dominated by pressure broadening. The effect of pressure broadening depends linearly on the pressure with a typical magnitude of 10 MHz torr^{-1} of gas. This result means that the total pressure in the Broida oven chamber (mainly argon carrier gas) has to be reduced to below 100 mtorr in order to obtain narrow lines and strong peak absorption coefficients. The solution to this problem is to increase the pumping speed by replacing the usual mechanical vacuum pump on the Broida oven with a Roots blower.

C. Molecular Beams

The Broida oven is a nearly ideal source for the spectroscopy of diatomic molecules and small polyatomic molecules such as CaOH. For larger species, however, the spectral congestion is too severe and the collisional relaxation rates are too high to record resonant, rotationally resolved spectra. The solution to this problem is to lower the temperature to eliminate the spectral congestion and to lower the pressure to eliminate the

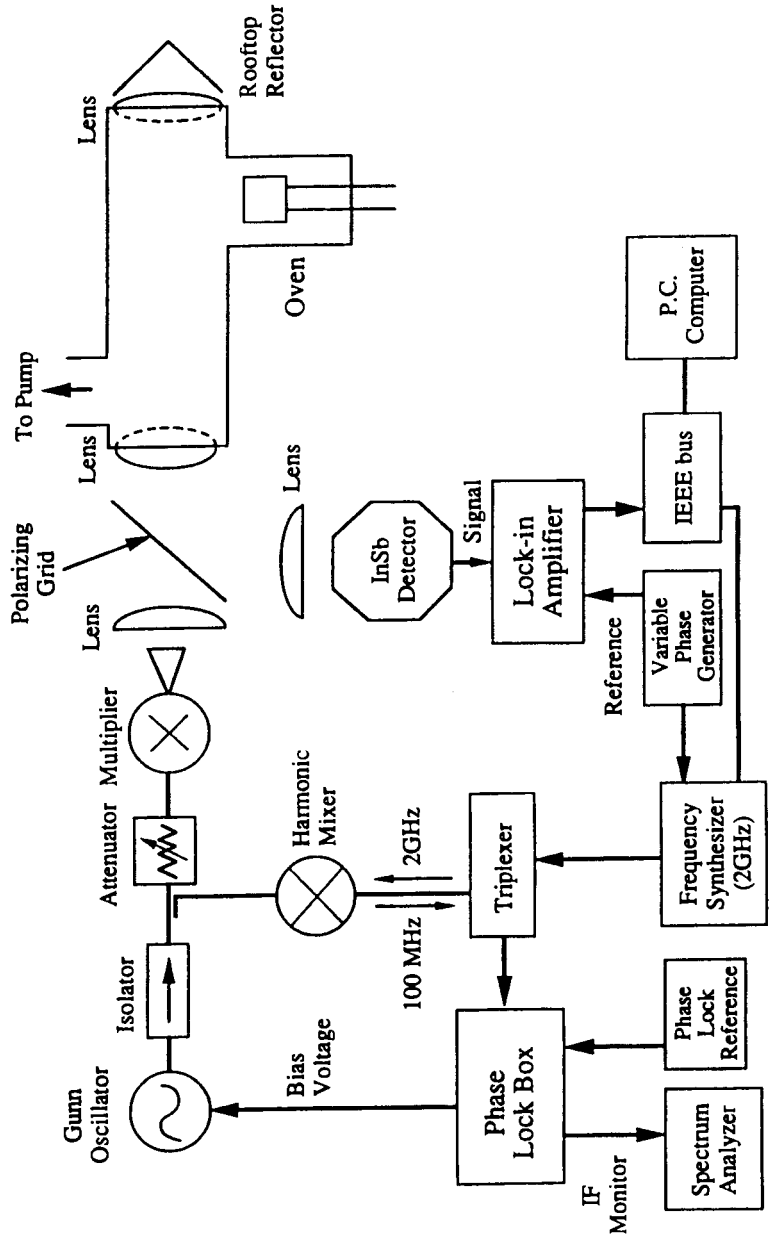

Figure 3. Block diagram of the millimeter wave spectrometer used by the Ziurys group. The instrument uses a phase locked Gunn oscillator as a source of radiation and an InSb detector. [Reprinted with permission from ref. 37. Copyright 1994 American Institute of Physics.]

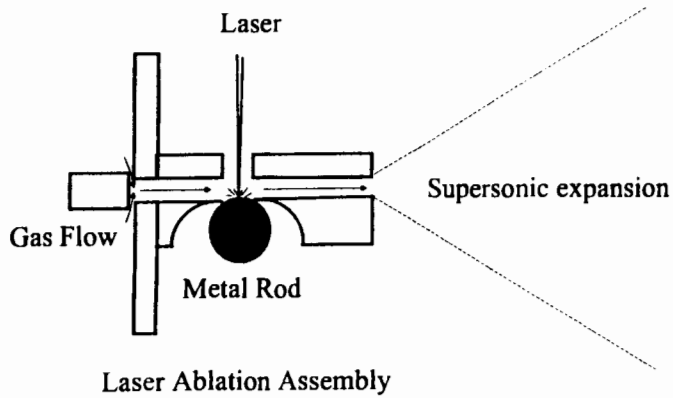

Figure 4. Laser ablation fixture used to make a supersonic molecular jet. The pulsed valve is synchronized with the ablation laser and the gaseous products expand into a vacuum and cool.

collision-induced redistribution of the excited-state population. A molecular beam source has these desirable properties.

The breakthrough experiment was carried out by Whitham et al. [39, 40] in France. They used a "Smalley-type" laser vaporization source (Fig. 4) to provide a molecular beam of Ca atoms entrained in He or Ar gas. The second harmonic (532 nm) from a pulsed Nd:YAG laser was focused (Fig. 4) on a rotating calcium rod. About 500 μs prior to this, a pulsed valve (left side of Fig. 4) is opened and the plume of vaporized metal is entrained in Ar or He gas. The carrier gas is seeded with a few percent of the oxidant such as H_2O. The plume of excited- and ground-state metal atoms are carried down a short channel and react with the oxidant. At the end of the channel, the product molecules such as CaOH expand into the vacuum chamber and cool. After a short expansion, the pressure has dropped so low that the molecules are effectively in a collisionless, ultracold (<10 K) environment.

The molecular jet of molecules is crossed with a tunable dye laser and the laser-induced fluorescence is collected with a lens and focused on a PMT detector (Fig. 5). In the original experiments, a standard pulsed dye laser was used to match the 10-Hz duty cycle of the pulsed valve and the pulsed Nd:YAG vaporization laser. Although this approach provides a high S/N ratio and wide spectral coverage, the resolution is limited by the laser line width of typically 0.5 cm^{-1} (no étalon) to 0.05 cm^{-1} with an étalon.

The simplest method to obtain high-resolution spectra is to replace the pulsed dye laser with a CW single-mode dye laser. As Steimle and co-workers have demonstrated in a series of beautiful experiments, this

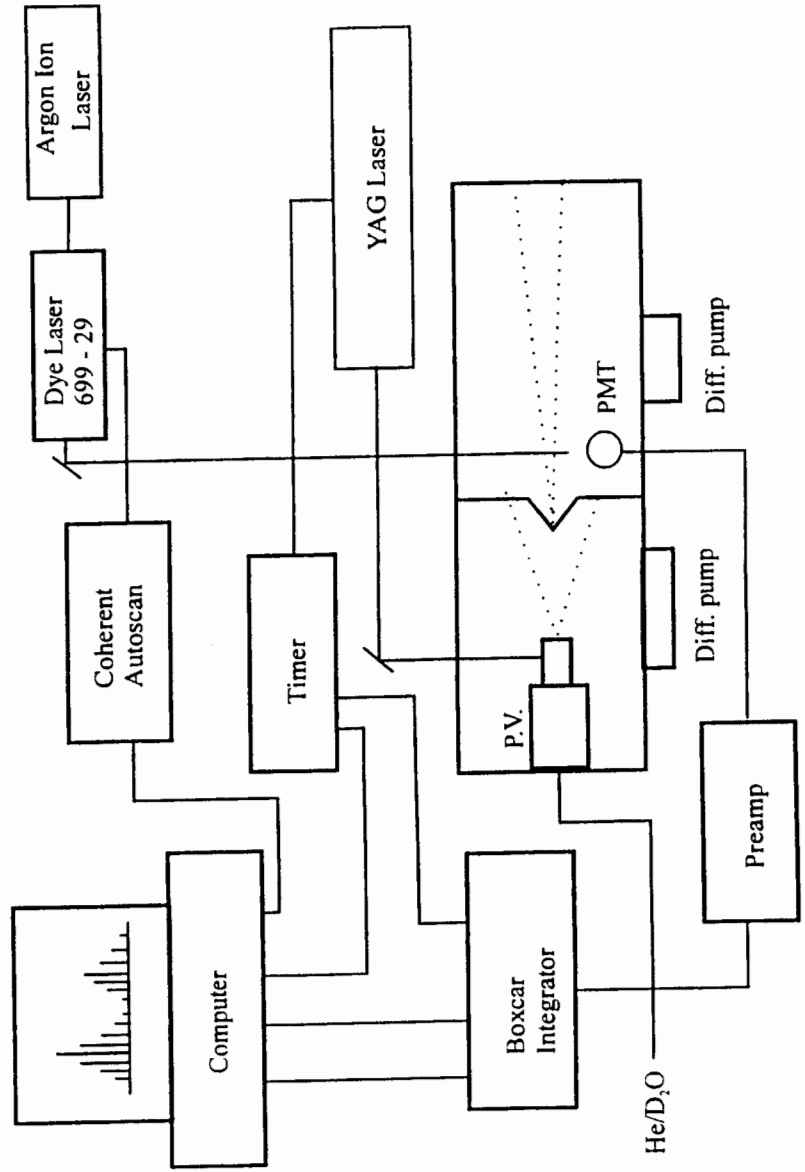

Figure 5. A block diagram of the laser ablation, molecular beam spectrometer at the University of Waterloo. [Reprinted with permission from ref. 74. Copyright 1996 Academic Press.]

technique is very effective. The main drawback is that most of the laser photons are wasted because of the duty cycle mismatch between the pulsed molecular beam source and the CW laser.

An alternate approach used by the Miller group is to pulse amplify a CW dye laser. This approach degrades the laser resolution from about 1 MHz to about 200 MHz but results in a high-power pulsed laser beam with excellent mode quality. This high peak power and high spectral resolution results in excellent spectra with an improved S/N ratio. The only serious drawback of this scheme is the increased complexity and cost of the laser systems.

There is one additional choice that needs to be made in setting up a pulsed molecular beam spectrometer. The laser beam can cross the molecular jet close ($\sim$1 cm) to the pulsed valve, as implemented by the Miller group. This technique gives a relatively large signal, but there is often a fluorescent background from the laser-vaporized plume of metal atoms (high signal/high noise). In this case, it is useful to use filters or a monochromator to isolate the laser-induced fluorescence signal. The alternative approach is to skim the jet (with either a true skimmer or a large hole) in order to form a molecular beam and to cross the laser and molecular beams at some distance ($\sim$10 cm) from the pulsed valve (Fig. 5). This arrangement gives a much reduced signal since the molecular concentration is dropping rapidly during the expansion but the fluorescent background is nearly eliminated (low signal/low noise). This latter approach is advocated by the Steimle group.

The application of molecular beam technology has resulted in the detailed rotational analysis of numerous larger alkaline earth derivatives such as CaC_5H_5. From the rotational analysis (and the improved vibrational analysis), one can infer molecular structure. In addition, large electric fields can be easily applied to molecular beams in order to measure dipole moments through the Stark effect. Dipole moments provide information about charge distributions. The alkaline earth derivatives are a unique family of molecules because so much detailed information is available for them. These simple one metal–one ligand molecules are useful as models for more complex species found in inorganic chemistry and surface science.

III. CHEMISTRY AND PHOTOCHEMISTRY

One of the surprising aspects of the chemistry of alkaline earth atoms is that ground-state atoms can react readily in the gas phase with molecules such as H_2O and CH_3OH. In solution, the overall reaction

$$Ca(s) + 2H_2O(\ell) \rightarrow Ca(OH)_2(s) + H_2(g) \qquad (4)$$

is vigorous. In the gas phase, however, the elementary reaction

$$Ca(g) + H_2O(g) \rightarrow CaOH(g) + H(g) \qquad (5)$$

does not occur because it is endothermic by 27 kcal mol^{-1}. The CaOH molecule obviously does form in a Broida oven and even chemiluminescence from the $\tilde{B}^2\Sigma^+$ and $\tilde{A}^2\Pi$ states can be seen. What is the source of this extra energy?

The laser excitation of Ca atoms to the $^3P_1$ state can provide an additional 44 kcal mol^{-1} of energy and the direct reaction

$$Ca(^3P_1) + H_2O(g) \rightarrow CaOH(g) + H(g) \qquad (6)$$

is now exothermic by 17 kcal mol^{-1}. Thus, the increased production of CaOH when Ca* is available is explained by the opening of the direct reaction channel (6). In a high-pressure CH_4/O_2 flame, there is also considerable energy available and many free radicals such as OH can react with Ca,

$$Ca(g) + OH(g) \rightarrow CaOH(g) \qquad (7)$$

in the presence of a third body. In a laser vaporization source, the plume of Ca atoms contains a large fraction of Ca* and Ca^+, which readily react to give CaOH in the molecular beam. Thus in many cases the deliberate or inadvertent presence of Ca* or OH accounts for the synthesis of CaOH. In a normal Broida oven, however, the thermal vaporization of Ca at about 1000°C yields a very low concentration of Ca*. It is found that the production of CaOH can be dramatically increased by simply increasing the total pressure in the chamber from 1 to 10 torr by decreasing the pumping speed. This fact points to a mechanism that needs a third body in a rate-controlling step.

Two possible mechanisms [41] are

Mechanism A

$$Ca + H_2O \xrightarrow{Ar} HCaOH \qquad (8)$$

$$HCaOH + Ca \rightarrow CaH + CaOH \qquad (9)$$

$$CaH + H_2O \rightarrow CaOH + H_2 \qquad (10)$$

$$2Ca + 2H_2O \rightarrow 2CaOH + H_2 \qquad (11)$$

or

Mechanism B

$$Ca + H_2O \xrightarrow{Ar} HCaOH \quad (8)$$

$$HCaOH + H_2O \rightarrow Ca(OH)_2 + H_2 \quad (12)$$

$$Ca(OH)_2 + Ca \rightarrow 2\,CaOH \quad (13)$$

$$2\,Ca + 2\,H_2O \rightarrow 2\,CaOH + H_2 \quad (11)$$

In these reactions, other alkaline earths can be substituted for Ca and other oxidants such as CH_3OH or HC(O)OH, which contain the OH group, can be substituted for H_2O.

Both mechanisms have as their first, and rate-controlling step, the insertion of a Ca atom into one of the O—H bonds of water. Additional support for the existence of an HCaOH intermediate comes from the matrix isolation experiments of Margrave and co-workers [14]. When Ca and H_2O were cocondensed in an argon matrix, a $Ca(H_2O)$ complex formed. Upon irradiation of the matrix with light near the metal resonance lines, the Ca atom inserted into H_2O and the infrared (IR) absorption of the HCaOH molecules was detected. Irradiation with UV light then gave the CaOH molecule.

Although we cannot directly detect HCaOH because it probably has a dissociative UV spectrum [14], we can detect another predicted reaction intermediate in some of our experiments. Mechanism A predicts that the CaH molecule will be present in the Broida oven, and with some oxidants we have detected it by laser-induced fluorescence. The CaH molecule is seen when carboxylic acids such as formic acid are used to make the monocarboxylates such as SrO_2CH [42]. Curiously, CaH is not detected [41] when water or alcohols such as CH_3OH are used to make alkoxides such as $CaOCH_3$. More experimental and theoretical work is necessary to establish the chemical mechanisms involved in the reactivity of the alkaline earth atoms.

There have been several studies of the reaction dynamics of the ground and excited states of the alkaline earth atoms with various oxygen-containing molecules under single collision conditions. Although these studies are not directly applicable to the multiple collision regime in the Broida oven, they clarify the dynamics of a single encounter between a metal atom and an oxidant molecule. Oberlander and Parson [43] looked at the reactions of Ca and Sr with water, alcohols, and peroxides. Similar studies

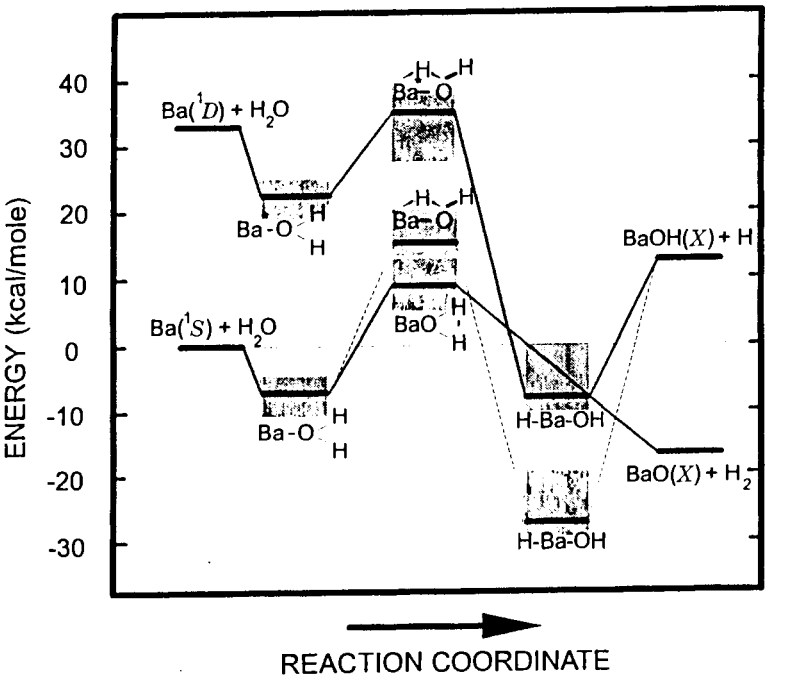

Figure 6. The reaction of Ba and H_2O. The reactions on the ground-state potential surface show the BaO (dashed) and BaOH (solid) product channels. On the excited $Ba(^1D) + H_2O$ surface only the BaOH channel is open. [Reprinted with permission from ref. 44. Copyright 1993 American Institute of Physics.]

of the reactivity of Ba were made by Davis et al. [44] as well as by de Pujo and co-workers [45–47]. The basic conclusions are illustrated in Figure 6.

The ground state of the Ba atom reacts with water by two different mechanisms [44] (Fig. 6). The main channel is the direct exothermic reaction that results in the products BaO and H_2. The minor channel (dotted lines) is the insertion of Ba into the OH bond (H migration) that results in the endothermic BaOH + H products. More than simple energetics is involved, however, because even when the Ba atom is given enough energy to overcome the insertion barrier, the reaction strongly favors the direct BaO product.

The reactivity of excited ^1D atoms with water is very different than the reactivity of the ground state Ba atoms (Fig. 6). The "diradical" character of the excited state strongly favors insertion to give the BaOH product

exclusively. Even though the BaO product is favored on energetic grounds, none is produced. The BaOH product angular distributions are consistent with an HBaOH intermediate. The reactions of Ca and Sr with H_2O and H_2O_2 follow a similar pattern, although the dynamics are postulated by Parson and co-workers [48,49] to be slightly different.

The reactions of Ca, Sr, and Ba with alcohols [43–45] are also different in that only the insertion channel is seen for both ground- and excited-metal atoms. The reaction intermediate is HMOR in all cases and the H atom leaves to give the MOR product. Very recently, the production of a small amount of CaOH was reported in the reaction of Ca with alcohols [50, 51]. The bulky R group suppresses the production of the energetically favored MO + HR products. Under both single collision and multiple collision conditions the most important dynamical event is the insertion of an alkaline earth metal atom in an H—OR bond.

It is presumed that the production of other monovalent derivatives such as $CaNH_2$ or CaC_5H_5 from NH_3 or C_5H_6 may involve similar excited metal atom insertions into N—H or C—H bonds. Unlike the reactions with H_2O and alcohols, however, no studies of the dynamics have been carried out and even the thermochemistry is very uncertain. Clearly, more experimental and theoretical work is necessary before any firm conclusions can be drawn about mechanisms.

IV. ELECTRONIC STRUCTURE

One of the most appealing aspects of the spectroscopy of the monovalent alkaline earth derivatives is that a simple, one-electron, hydrogenic model provides a reasonable picture of the electronic structure. This simple model is not usually applicable to the derivatives of the other elements of the periodic table. In fact, the major impediment to extending the work to the more chemically interesting transition elements is that the spectra will be difficult to interpret because of the presence of many states with large spin and orbital angular momenta.

The electronic structure can best be explained with a correlation diagram for Ca^+, CaF, and $CaNH_2$ as shown in Figure 7. The $CaNH_2$ molecule is ionic like Ca^+F^- so the electronic distribution can be approximated as $Ca^+NH_2^-$. The $CaNH_2$ molecule is planar with C_{2v} symmetry, not pyramidal like NH_3. The Ca^+ ion is isoelectronic with K, and has a ^2S ground state with low-lying ^2D and ^2P states. The approach of an F^- ligand changes the atomic ground state into a $4s\sigma\, X^2\Sigma^+$ molecular state in CaF.

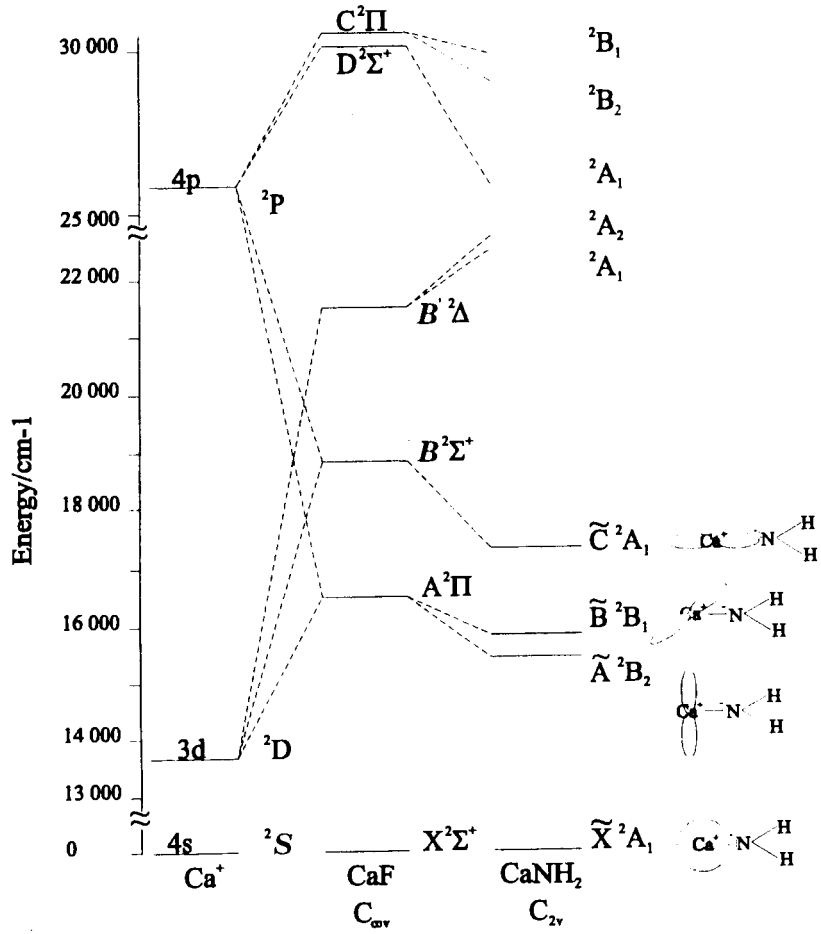

Figure 7. Correlation diagram of the low-lying states of Ca^+, CaF, and $CaNH_2$ [53].

The effect of the F^- ligand on the Ca^+ excited states is more complicated. The threefold orbital degeneracy of the ^2P state is partly lifted to give $4p\sigma$ and $4p\pi$ orbitals that correlate mainly with the $B^2\Sigma^+$ and $A^2\Pi$ states of CaF, respectively. For a ^2D atomic state, one obtains $3d\sigma$, $3d\pi$, and $3d\delta$ orbitals and $^2\Sigma^+$, $^2\Pi$, and $B'^2\Delta$ molecular states. In addition to lifting the degeneracy, the F^- ligand shifts the location of the states, stabilizing the Ca^+ ^2P states more than the ^2D states. Since the atomic l quantum number is no longer good in a molecule, some mixing of atomic orbitals also occurs.

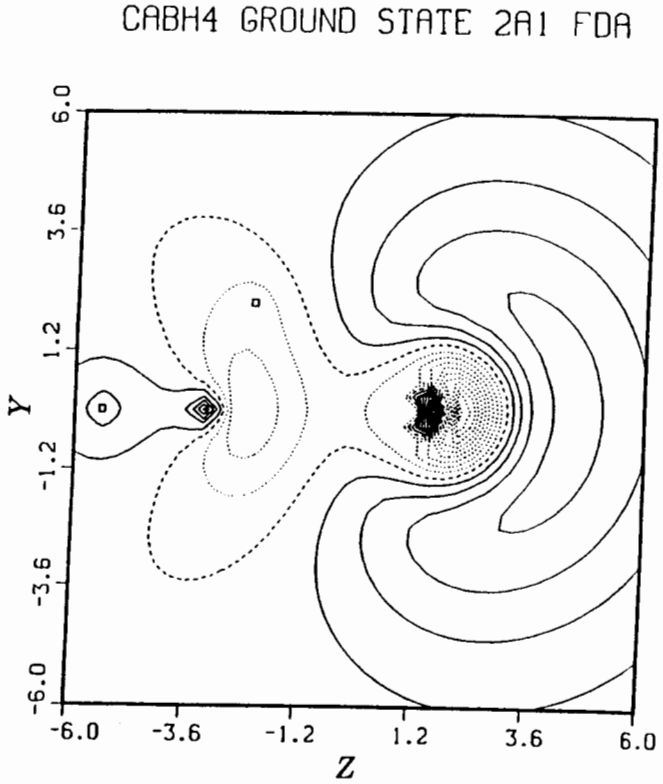

Figure 8. The $\tilde{X}^2A_1$ Feynman Dyson amplitude of $CaBH_4$ [55]. The Ca atom is to the right and the in-plane BH_2 part of the BH_4 group is to the left. [Reprinted from ref. 55, with kind permission from Elsevier Science-NL, Sara Burgerhartstraat 25, 1055 KV Amsterdam, The Netherlands.]

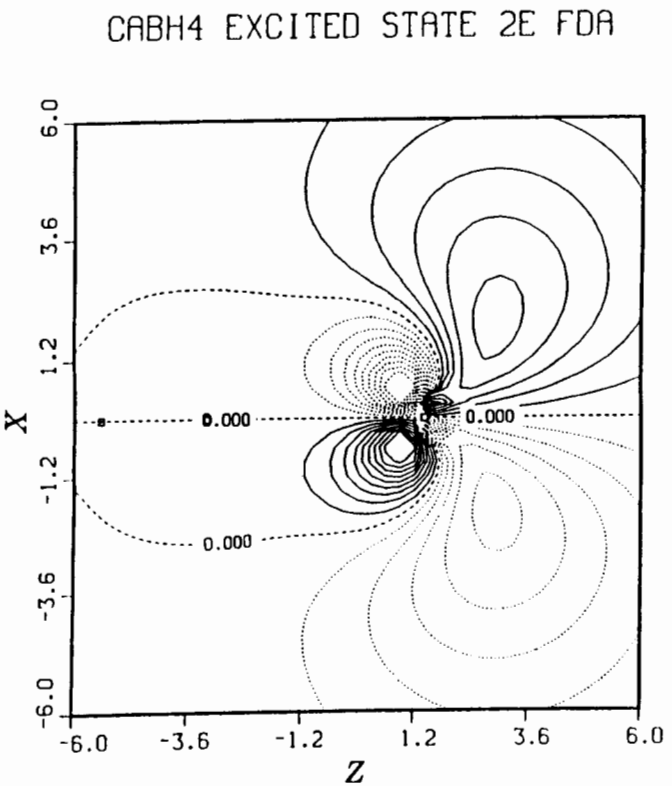

Figure 9. The $\tilde{A}^2E$ Feynman-Dyson amplitude of $CaBH_4$ [55]. [Reprinted from ref. 55, with kind permission from Elsevier Science-NL, Sara Burgerhartstraat 25, 1055 KV Amsterdam, The Netherlands.]

In particular, the $A^2\Pi$ state in CaF is about 70% $4p\pi$ and 30% $3d\pi$, while the $B^2\Sigma^+$ state is nearly a 50:50 mixture of $4p\sigma$ and $3d\sigma$ atomic orbitals [52]. This orbital mixing distorts the molecular orbitals in such a way as to keep the unpaired electron as far away as possible from the F^- ligand.

For simplicity, the $A^2\Pi$ state and $B^2\Sigma^+$ state of CaF can be considered to be three pure p orbitals, p_x, p_y for the $A^2\Pi$ state and p_z for the $B^2\Sigma^+$ state. If the F^- ligand is changed to NH_2^-, then the degeneracy of the p_x and p_y orbitals is lifted. From a high-resolution rotational analysis of the $\tilde{A}$–$\tilde{X}$ transition, the first excited state is the in-plane p_y orbital of b_2 symmetry. In Figure 7, the $CaNH_2$ is considered to lie in the plane of the paper so the $\tilde{B}^2B_1$ state is the p_x orbital out of the plane of the molecule (and the paper). The $\tilde{C}^2A_1$ state is now approximated by the p_z orbital. The $\tilde{A}$–$\tilde{X}$, $\tilde{B}$–$\tilde{X}$, and $\tilde{C}$–$\tilde{X}$ transitions of $CaNH_2$ can be approximated as the $4p$ $(p_x, p_y, p_z) \leftarrow 4s$ resonance transition of Ca^+ perturbed by the presence of an NH_2^- ligand.

These qualitative predictions are clearly too simple but they provide a useful "zeroth-order" model of the electronic structure. For example, the model predicts values for the spin-rotation parameters in the $\tilde{A}$, $\tilde{B}$, and $\tilde{C}$ states of $CaNH_2$ that are in reasonable agreement with experiment [53]. The qualitative predictions of molecular properties can also be compared with the results of ab initio calculations. The first calculations on $CaNH_2$ [54] and related molecules such as $CaBH_4$ were made by Ortiz

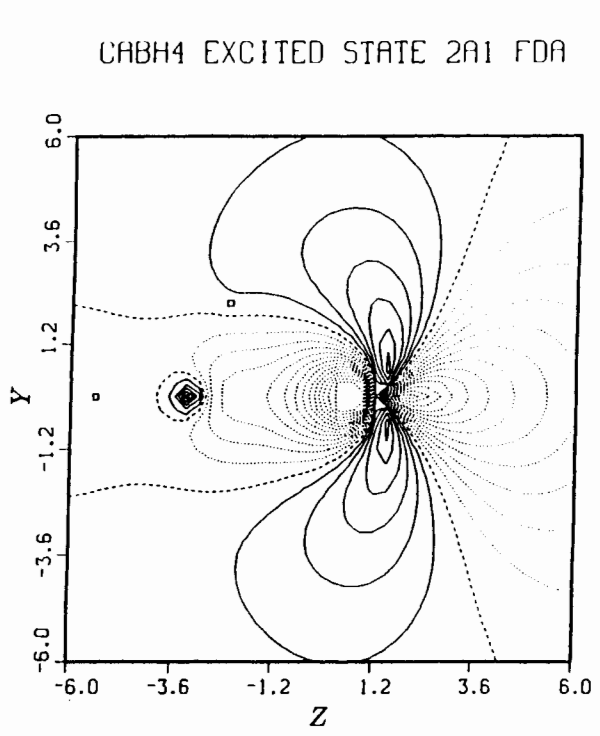

Figure 10. The $\tilde{B}^2A_1$ Feynman–Dyson amplitude of $CaBH_4$. [Reprinted from ref. 55, with kind permission from Elsevier Science-NL, Sara Burgerhartstraat 25, 1055 KV Amsterdam, The Netherlands.]

[55–57] and his results are in general agreement with the simple one-electron picture.

The ab initio electron propagator calculations of Ortiz [54–57] give "Feynman–Dyson amplitudes," which are analogous to orbitals in more conventional calculations. For the $CaBH_4$ molecule [55], the ground $\tilde{X}^2\Sigma^+$ state (Fig. 8) has the general appearance of a distorted $4s\,Ca^+$ orbital. The $Ca^+BH_4^-$ molecule has C_{3v} symmetry with the Ca^+ ion (to the right in Fig. 8) bonding to the face of the BH_4^- tetrahedron. In these plots, the solid lines are the positive wave function contours while the dotted lines are negative. Nodal surfaces are indicated by dashed lines. In Figure 9, a similar plot for the first excited ^2E state is presented. This ^2E state correlates to the $A^2\Pi$ state of CaF and the $\tilde{A}^2B_2$ and $\tilde{B}^2B_1$ states of $CaNH_2$ (Fig. 7). Notice that the orbital containing the unpaired electron is a distorted $4p$ orbital. Finally, in Figure 10, the second excited $^2A_1$ state, which correlates to the $B^2\Sigma^+$ state of CaF and the $\tilde{C}^2A_1$ state of $CaNH_2$, is a heavily mixed $4p\sigma$, $3d\sigma$ orbital.

V. SURVEY OF MOLECULES

A. Monohydroxides, MOH

The alkaline earth monohydroxides are the most studied of all of the molecules discussed in this chapter because they are easy to make and are relatively simple to study. Since the early literature has already been reviewed [28], mainly the more recent (since ~ 1990) work will be discussed.

The Ziurys laboratory has recorded the millimeter wave pure rotational spectra for MgOH [23, 58–60], MgOD [60, 61], CaOH [58, 59, 62], CaOD [61], SrOH [58, 59, 63], SrOD [63], BaOH [58, 59, 64], and BaOD [64]. The spectra are simple and show the spin-rotation doublets in the $\tilde{X}^2\Sigma^+$ ground state (Fig. 11) as well as numerous vibrational satellites. A typical spin doublet is shown for the MgOH $N = 13 \leftarrow 12$ transition [23]. The alkaline hydroxides have low-lying vibrational states (Fig. 12) that are populated in the Broida oven and give rise to numerous vibrational satellites as shown in a stick diagram in Figure 13.

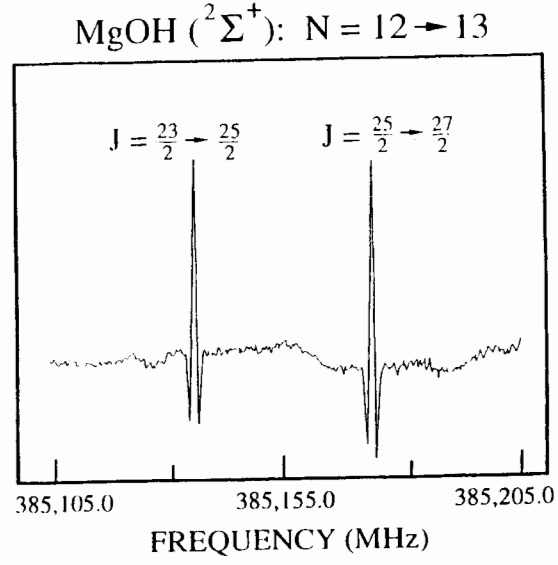

Figure 11. The $N = 13 \leftarrow 12$ rotational transition of ground-state MgOH. The splitting is due to the spin–rotation interaction in the $\tilde{X}^2\Sigma^+$ state. [Reprinted from ref. 23, with kind permission from Elsevier Science-NL, Sara Burgerhartstraat 25, 1055 KV Amsterdam, The Netherlands.]

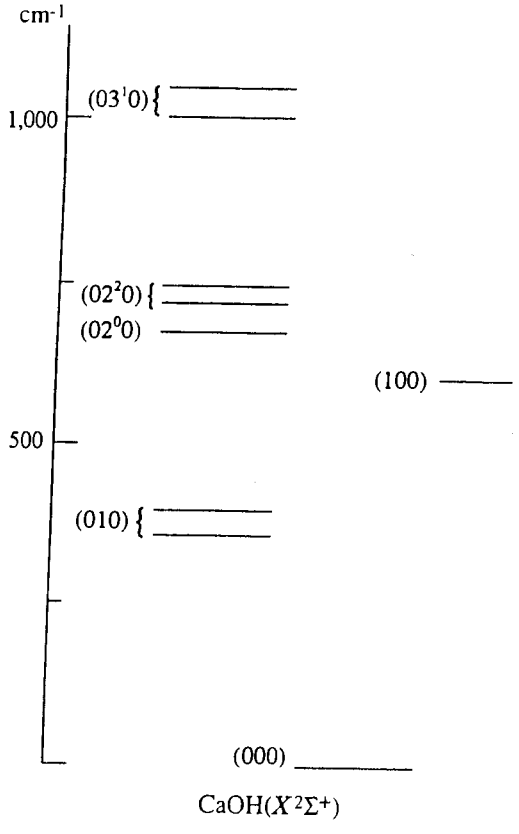

Figure 12. The low-lying vibrational levels of the CaOH $\tilde{X}^2\Sigma^+$ electronic state. [Reprinted with permission from ref. 58. Copyright University of Chicago Press.]

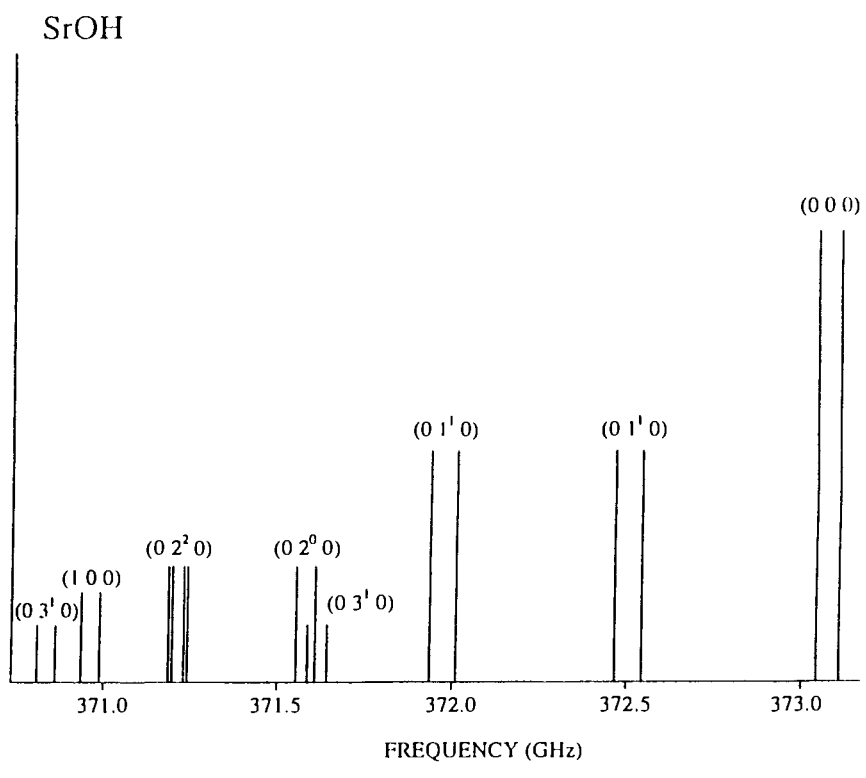

Figure 13. A stick diagram of the vibrational satellite transitions associated with the $N = 25 \leftarrow 24$ rotational transition of SrOH. [Reprinted with permission from ref. 58. Copyright University of Chicago Press.]

The high-quality pure rotational data, combined with the earlier measurements of the vibrational intervals by laser spectroscopy, allows an improved molecular geometry to be determined. For MgOH, CaOH, SrOH, and BaOH, the geometries are linear in the ground state although the bending potentials [60] are very flat (Fig. 14). Although quasilinear behavior has been ruled out for the heavier members of the family, the situation is more ambiguous for BeOH. The latest ab initio calculations [65] do not predict a barrier to linearity for BeOH in the ground state, in agreement with a linear structure proposed on the basis of electron spin resonance (ESR) experiments by Brom and Weltner [11]. Table 1 gives the r_0 bond lengths for the alkaline earth monohydroxides. The values for BeOH are the r_e predictions of an ab initio calculation by Fernandez [65]. Note that the first excited electronic state of MgOH [66] and the $\tilde{F}$ state of CaOH [67] have bent geometries.

Millimeter wave spectroscopy with a free space cell such as a Broida oven is more sensitive than lower frequency microwave spectroscopy. However, the higher J transitions monitored by millimeter wave spectroscopy often do not show the effects of hyperfine structure. In the case of CaOH and SrOH, the proton hyperfine structure was measured in beautiful pump–probe microwave optical double resonance experiments in the Steimle group [24, 68]. They adapted the classic atomic beam magnetic resonance experiments to work with a pulsed laser vaporization source and replaced the microwave fields in the A and C regions by optical fields (Fig. 15). These sensitive, high-precision measurements yielded a very small value for the proton Fermi contact parameter (b_F), consistent with ionic bonding and a

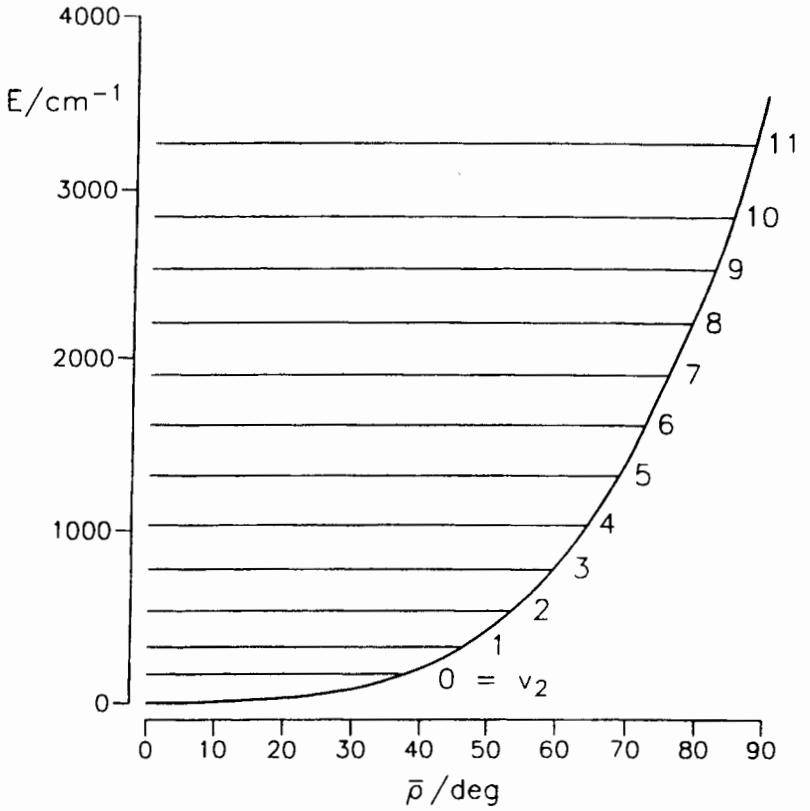

Figure 14. The bending potential energy function of MgOH. [Reprinted from ref. 60, with kind permission from Elsevier Science-NL, Sara Burgerhartstraat 25, 1055 KV Amsterdam, The Netherlands.]

TABLE 1 Bond Lengths (r_0) for MOH Molecules (in Å)

Molecule	r_{MO}	r_{OH}
BeOH[a]	1.378	0.944
MgOH[b]	1.780	0.871
CaOH[b]	1.985	0.922
SrOH[b]	2.111	0.922
BaOH[b]	2.200	0.927

[a]Ab initio r_e values in [65].
[b]Reference 61.

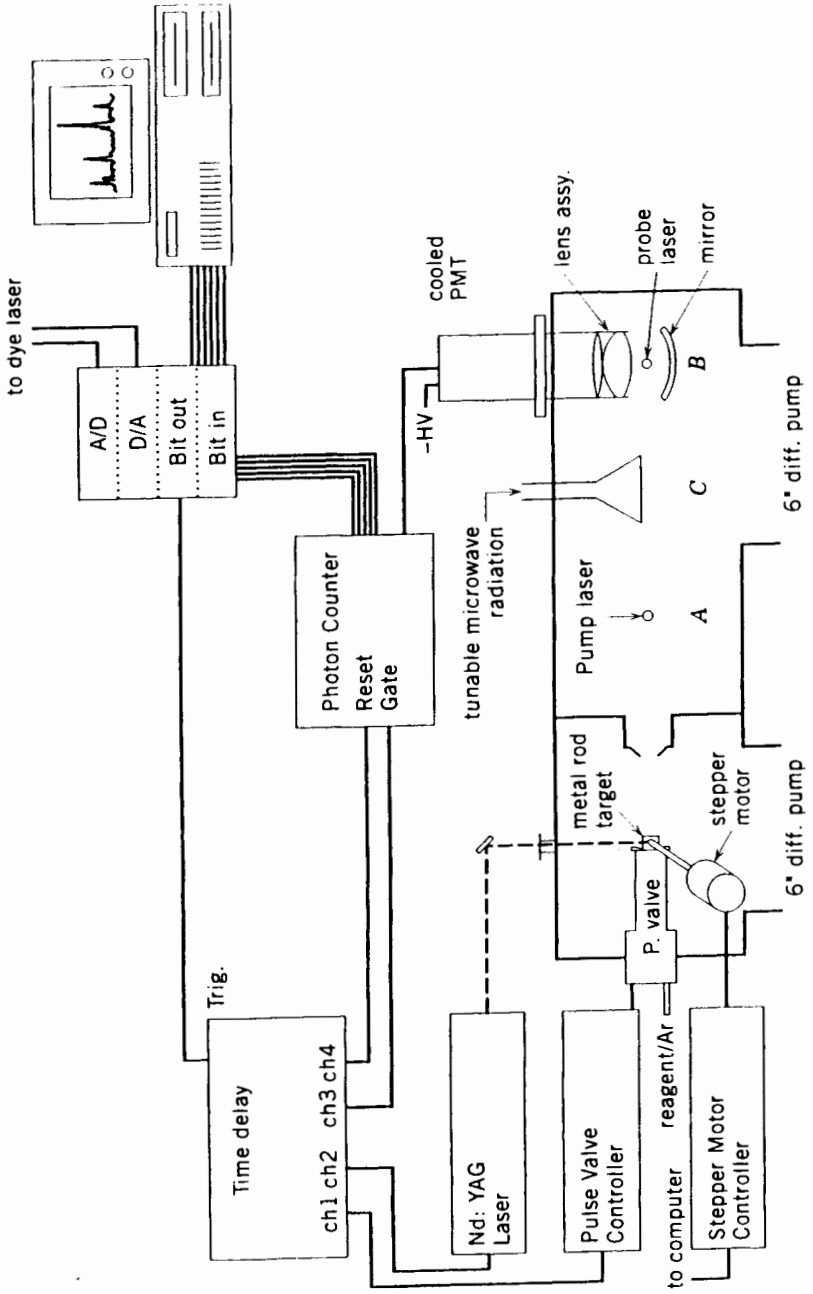

Figure 15. The pulsed molecular beam spectrometer used to record the microwave spectrum of CaNC [108] and CaOH [24]. [Reprinted from ref. 108. Copyright 1994 American Institute of Physics.]

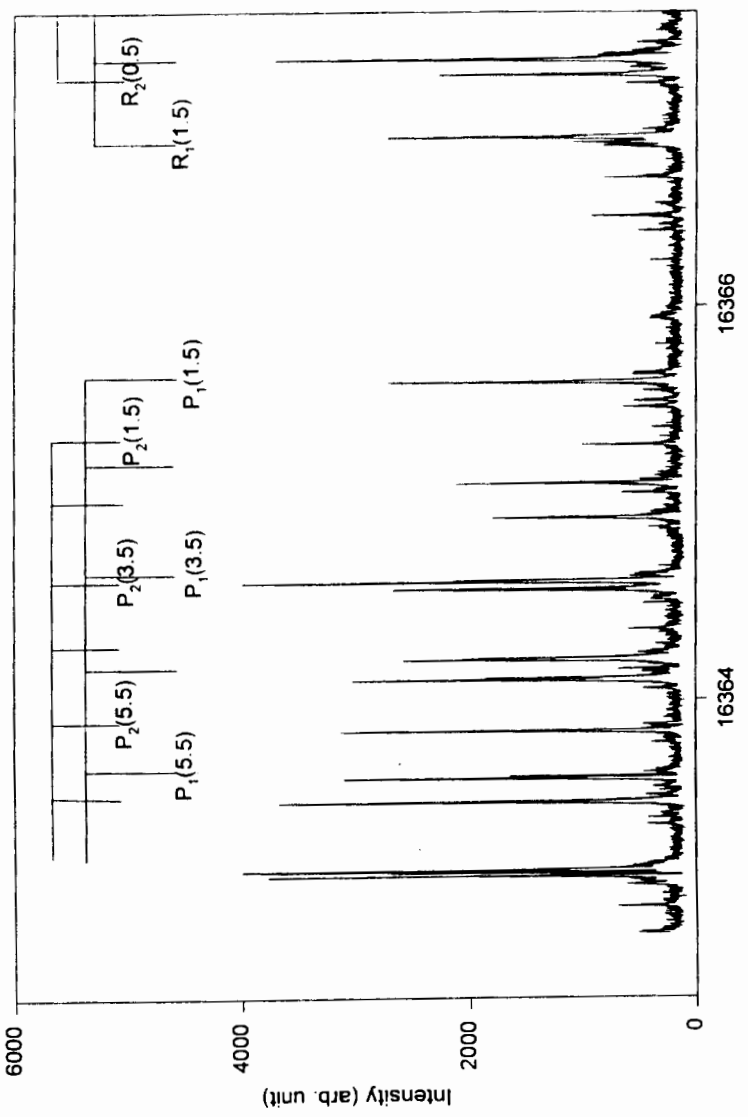

Figure 16. Laser excitation spectrum of the 000–000 band of the $\tilde{B}^2\Sigma^+ - \tilde{X}^2\Sigma^+$ transition of SrOD. [Reprinted with permisssion from ref. 74. Copyright 1996 Academic Press.]

closed-shell OH^- ligand. In general, hyperfine structure is very valuable because the hyperfine parameters are determined by the electron distribution.

The Steimle group also measured the dipole moments of CaOH and SrOH in a molecular beam Stark experiment [69]. The surprisingly low values of 1.465 and 1.900 D in the ground $\tilde{X}^2\Sigma^+$ state for CaOH and SrOH, respectively, were found, in moderate agreement with the ab initio calculation of 0.98 D for CaOH [70]. The semiempirical predictions of Mestdagh and Visticot [71] are in good agreement with experiment and explain the small values. The semiempirical scheme is a modified electrostatic Rittner model that allows for the effect of the unpaired electron on the opposite side of the metal away from the OH^- ligand (cf. Fig. 8). In other words, the large $Ca^{2+}OH^-$ dipole is nearly canceled by the dipole created by the unpaired electron on the opposite side of the Ca^{2+} atom. A ligand field treatment of the bonding is also available [72].

In recent years, the optical spectroscopy of the metal hydroxides has also bloomed with new analyses of the 0–0 bands of the $\tilde{B}^2\Sigma^+ - \tilde{X}^2\Sigma^+$ transitions of CaOD [73], SrOD [74], and BaOH [47]. The use of a cold molecular beam source results in a simple spectrum and in narrower lines as illustrated in Figure 16 for SrOD [74].

TABLE 2 Vibrational Frequencies for MOH and MOD Molecules (in cm^{-1})

Molecules	ν_1(O—H stretch)	ν_2(M—O—H bend)	ν_3(M—O stretch)
MgOH		160[a]	750[a]
MgOD		~118[a]	
CaOH	3778[b]	353[c]	609[d]
CaOD	2790[b]	267[e]	605[d]
SrOH		364[f]	527[g]
SrOD		~282[h]	517[i]
BaOH		342[j]	492[j]
BaOD		258[i]	482[j]

[a]Reference 60.
[b]Reference 67.
[c]Reference 85.
[d]Reference 81.
[e]Reference 83.
[f]Reference 77.
[g]Reference 75.
[h]Reference 33.
[i]Reference 74.
[j]Reference 86.

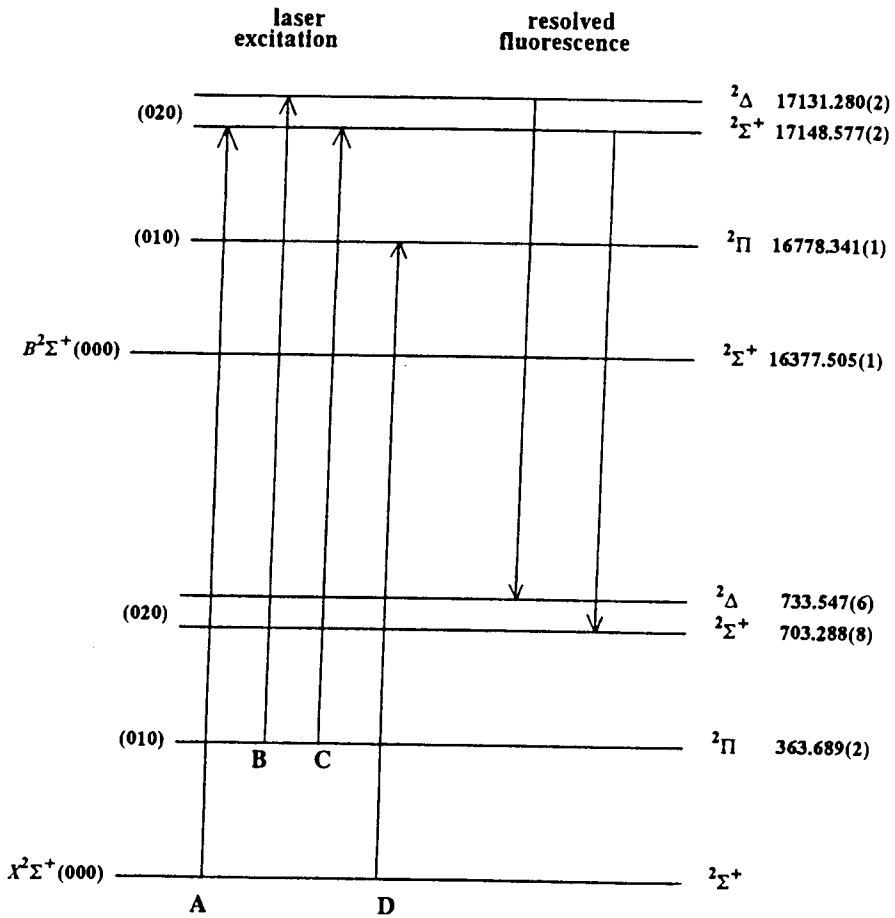

Figure 17. Laser excitation spectra (up arrows) and dispersed laser-induced fluorescence spectra (down arrows) of the $\tilde{B}^2\Sigma^+-\tilde{X}^2\Sigma^+$ transition of SrOH. [Reprinted with permission from ref. 77. Copyright 1993 NRC Research Press.]

The majority of the work, however, has been carried out in a Broida oven by Coxon and co-workers [75–84]. They concentrated on the study of the vibrational intervals in the ground $\tilde{X}^2\Sigma^+$ states (Table 2) and in understanding the vibronic interactions in the $\tilde{A}^2\Pi$ states. As illustrated in Figure 17, the combination of laser excitation spectroscopy and dispersed laser-induced fluorescence allows the vibronic levels to be mapped out. The $\tilde{A}^2\Pi$ states suffer from the combined influence of the Renner-Teller effect, Fermi resonance and spin–orbit coupling. The Coxon group recorded a large

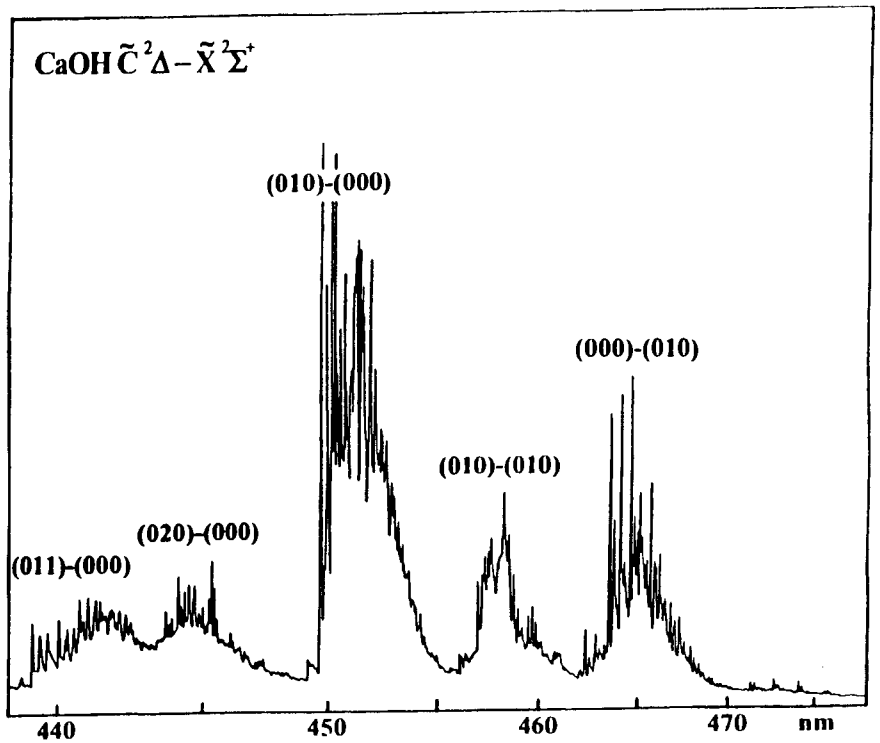

Figure 18. Laser excitation spectrum of the $\tilde{C}^2\Delta-\tilde{X}^2\Sigma^+$ transition of CaOH. [Reprinted with permission from ref. 85. Copyright 1992 American Institute of Physics.]

number of bands in the $\tilde{B}-\tilde{X}$ and $\tilde{A}-\tilde{X}$ transitions of SrOH [75–77], CaOH, and CaOD [78–84].

The Herzberg–Teller effect is another name for the vibronic coupling of electronic and vibrational motion. This effect was used by Jarman and Bernath [85] to locate the missing $\tilde{C}^2\Delta$ state in CaOH via the forbidden $\tilde{C}^2\Delta-\tilde{X}^2\Sigma^+$ transition. In this case, the 0–0 band remains forbidden but the interaction between the bending motion and the electronic motion in the $\tilde{C}^2\Delta$ state make bands such as 010–000 weakly allowed (Fig. 18). The $\tilde{C}^2\Delta$ state also displays the Renner–Teller effect, which is the interaction of vibrational angular momentum with orbital angular momentum in a linear molecule. There is some evidence for a low-lying $\tilde{A}^2\Delta$ state in the spectrum of BaOH, again through the effects of vibronic coupling [86].

Spectroscopic efforts have concentrated on the $\tilde{A}^2\Pi-\tilde{X}^2\Sigma^+$ and $\tilde{B}^2\Sigma^+-\tilde{X}^2\Sigma^+$ transitions of the MOH molecules although these transitions for

BeOH and MgOH (along with $\tilde{A}-\tilde{X}$ transition of BaOH) are in need of rotational analysis. Very little work is available for other more highly excited states, except in the case of CaOH. Jarman and Bernath [85] located the $\tilde{C}^2\Delta$ state of CaOH and very recently Pereira and Levy [67] found the $\tilde{D}^2\Sigma^+$, $\tilde{E}^2\Sigma^+$, and $\tilde{F}$ states at 28,153, 29,879, and 30,215 cm^{-1}, respectively. In these experiments, pulsed lasers were used with a pulsed laser vaporization source. The $\tilde{F}$ state is the first bent covalent state to be identified for CaOH and it correlates with the $C^2\Pi$ state of CaF (Fig. 7). The first unambiguous measurement of the OH and OD stretching frequency (Table 2) was also possible because of the favorable Franck–Condron factors in the $\tilde{F}$ (bent) $\rightarrow \tilde{X}$ (linear) transition.

There are also some unpublished optical–optical double resonance data on the $\tilde{G}^2\Pi$ state of CaOH at 32,630 cm^{-1} [87]. The $\tilde{G}^2\Pi$ state correlates with the $E'^2\Pi$ state of CaF. In this work on CaOH (and CaOD), a number of vibronic states were observed for which vibrational assignments are difficult. Similar problems were found by Pereira and Levy [67] for some of their bands.

B. Monoalkoxides, MOR

The first alkaline monoalkoxides were prepared by Wormsbecher and Suenram [88] in 1982. They reacted Ca and Sr vapors with methylnitrite (CH_3ONO) in a Broida oven and detected the $\tilde{A}^2E-\tilde{X}^2A_1$ and $\tilde{B}^2A_1-\tilde{X}^2A_1$ transitions of $CaOCH_3$ and $SrOCH_3$. Close similarities with the CaOH and SrOH spectra were noted. Studies of the $\tilde{A}-\tilde{X}$ and $\tilde{B}-\tilde{X}$ transitions of a number of additional alkoxides such as $MOCH_2CH_3$, $MOC(CH_3)_3$, and so on, were published by Brazier et al. [41] for M = Ca, Sr, and Ba. The rotational analysis of the $\tilde{A}^2E_{3/2}-\tilde{X}^2A_1$ transition [89] proved that $SrOCH_3$ has C_{3v} symmetry with an Sr—O bond length of 2.12 Å in the ground state (cf. Table 1). Additional rotational analyses of $CaOCH_3$ are in progress by Brown [90] and co-workers at Oxford and in the Bernath group [91] at Waterloo.

The alkoxides are the only family of molecules in addition to the monohydroxides for which studies of the molecular dynamics of the formation reactions are available. Davis et al. [44] compared the reactivity of Ba (^1S and ^1D) atoms with water and methanol using crossed molecular beams. Similar experiments with Ba (^1P) atoms with many additional alcohols were published by de Pujo et al. [45]. Alcohols always yielded BaOR products, not the energetically favorable BaOH or BaO molecules. Oberlander and Parsons [43] extended these studies to Ca and Sr metals using a beam-gas configuration. Surprisingly Esteban et al. [50] were able to measure a very small amount of CaOH from the reaction of Ca* with alcohols.

C. Monocarboxylates, MO_2CR

The low-resolution spectra of Ca and Sr monoformate and monoacetate were first reported in 1985 [42]. A more extensive study of the formates, acetates, propionates, and butanoates [92] appeared in 1990 (Fig. 19). Calcium monoformate is believed to have C_{2v} symmetry with bidentate bonding. The spectra show three electronic transitions similar to $CaNH_2$

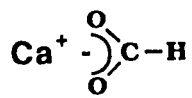

(Fig. 7) but it is speculated that the first excited $^2A_1$ state lies below the $^2B_1$, $^2B_2$ pair of states, which correlate to the $A^2\Pi$ state of CaF. Theoretical work and high-resolution analyses need to be carried out on the monocarboxylates to verify the ordering of the electronic states.

D. Monoformamidates, MO(NH)CH

Isoelectronic analogies are very helpful in understanding the geometry and electronic structure of the monovalent alkaline earth derivatives. For example, formamide, $HC(O)NH_2$, differs from formic acid, HC(O)OH, by the substitution of an NH_2 group for OH. The use of formamide as an oxidant in a Broida oven gives rise to a spectrum [93] with three electronic transitions $\tilde{A}-\tilde{X}$, $\tilde{B}-\tilde{X}$, and $\tilde{C}-\tilde{X}$ (Fig. 20) very similar to the corresponding monoformate derivatives.

It seems likely that the calcium and strontium monoformamidates have bidendate bonding of the ligand similar to the monoformate derivatives.

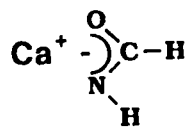

The formamidate anion differs from the formate anion by the isoelectronic substitution of an NH group for O. The metal–ligand

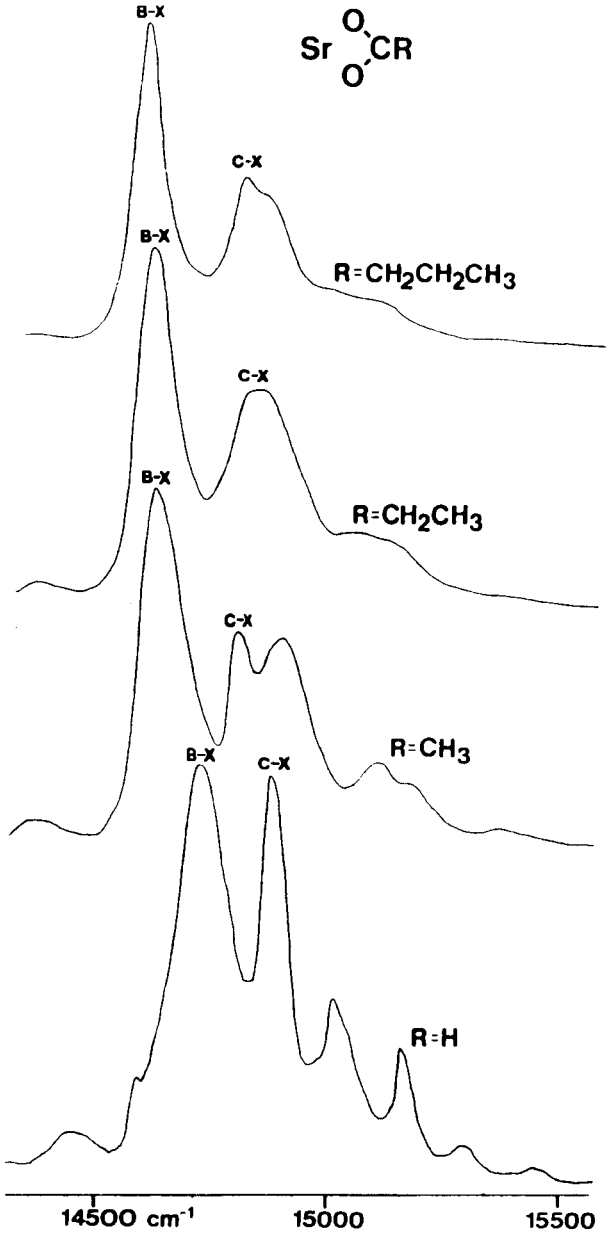

Figure 19. The laser excitation spectra of the $\tilde{B}-\tilde{X}$ and $\tilde{C}\ \tilde{X}$ transitions of the strontium monocarboxylate molecules. [Reprinted with permission from ref. 92. Copyright 1990 American Chemical Society.]

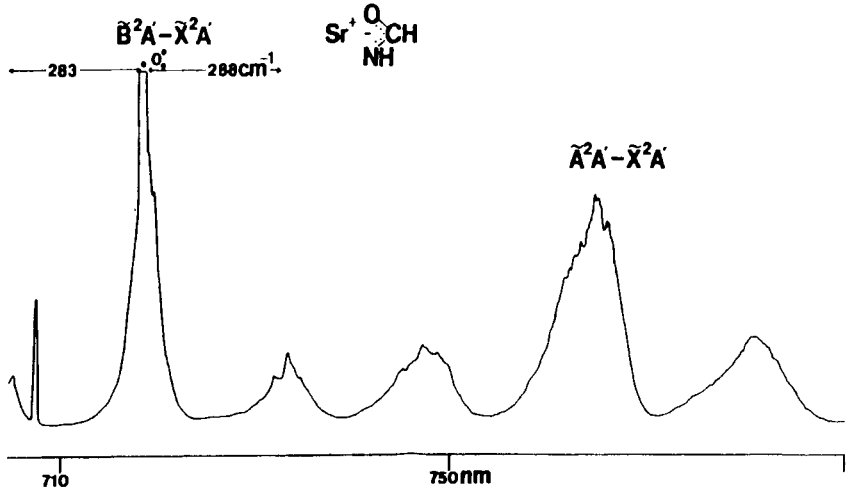

Figure 20. The dispersed fluorescence spectrum of the $\tilde{A}\ \tilde{X}$ and $\tilde{B}-\tilde{X}$ transitions of SrOC(NH)H. The laser is exciting the 0–0 band of the $\tilde{B}-\tilde{X}$ transition. [Reprinted with permission from ref. 93. Copyright 1990 American Chemical Society.]

vibrational frequencies of 351 and 288 cm^{-1} in the ground state for the calcium and strontium monoformamidates [93] are similar to the values (349 and 275 cm^{-1}, respectively) for the corresponding monoformates [92]. Again high-resolution spectra and theoretical calculations would be very helpful in confirming the assignments of the low-resolution spectra. Interestingly, while formamidate salts are unknown in normal inorganic chemistry (formates are common), they form readily in the gas phase.

E. Monoisocyanates, MNCO

The spectra of CaNCO and SrNCO were first reported in 1986 based on a low-resolution analysis of the products of the reaction of Ca and Sr with HNCO [94]. The $\tilde{A}^2\Pi-\tilde{X}^2\Sigma^+$ and $\tilde{B}^2\Sigma^+-\tilde{X}^2\Sigma^+$ transitions were clearly due to a linear molecule (cf. CaF in Fig. 7). For NCO derivatives, there is the possibility of linkage isomers. In the initial paper [94], we guessed that the oxygen-bonding structures, MOCN, were lowest in energy (cyanates), but this proved to be erroneous. The NCO ligand binds to Ca and Sr through the N atom to give metal isocyanates.

To determine the structure of CaNCO and SrNCO, a rotational analysis of the $\tilde{A}^2\Pi-\tilde{X}^2\Sigma^+$ transition of the SrNCO molecule was carried out [95].

TABLE 3 Calculated Bond Lengths for CaNCO, CaNNN, and CaNCS (in Å)[a]

Bond Distance	CaNCO	CaNNN	CaNCS
r(CaN)	2.194	2.177	2.247
r(NC or NN)	1.218	1.211	1.215
r(CO, NN, or CS)	1.199	1.188	1.596

[a]Reference 97.

By fixing the N—C bond length to 1.19 Å and the CO bond length to 1.23 Å, the Sr—N bond length of 2.26 Å was determined from the rotational constant (0.04258 cm^{-1}) in the $\tilde{X}^2\Sigma^+$ state. A rotational analysis [96] of the corresponding $\tilde{A}^2\Pi - \tilde{X}^2\Sigma^+$ transition of SrN_3 gave an identical Sr—N bond length when the N—N bond lengths in the N_3^- ligand were fixed to 1.18 Å. For SrNCO and SrN_3 to have identical metal–ligand bond lengths is consistent only with an isocyanate structure for SrNCO.

The corresponding rotational analyses have not yet been carried out for CaNCO and CaN_3 but some ab initio predictions [97] have been made by Chan and Hamilton (Tables 3 and 4). These calculations used the same 6–31 + G^* basis set used by Ortiz [54] and are at the $MP2$ level. There is good agreement between the calculated vibrational frequencies and the experimental values (Table 4). The vibrational frequencies of NCO^- in the solid state are 2182, 1211, and 631 cm^{-1} to be compared with the calculated values of 2191, 1327, and 826 cm^{-1} for ν_1, ν_2, and ν_4, respectively (Table 4). No laboratory spectra are available for CaNCS.

F. Monoazides, MN_3

The isoelectronic NCO^- and N_3^- anions are often called pseudohalides because they have a chemistry similar to that of F^-, Cl^-, Br^-, and I^-. In a similar fashion, we find that CaN_3, SrN_3, CaNCO, and SrNCO all have similar spectra and that the electronic structure resembles that of CaF (Fig. 7). As in "regular" chemistry, chemical and isoelectronic analogies are a powerful tool for interpreting our gas-phase inorganic chemistry.

The CaN_3 and SrN_3 molecules were made in a Broida oven by the reaction of Ca and Sr vapors with hydrazoic acid, HN_3 [96]. The reaction is relatively vigorous and, in contrast to the other Ca and Sr reactions, exciting the atomic $^3P_1$ state of the metal increases the reactivity only slightly. The $\tilde{B}^2\Sigma^+ - \tilde{X}^2\Sigma^+$ and $\tilde{A}^2\Pi - \tilde{X}^2\Sigma^+$ transitions could be identified

TABLE 4 Calculated and Observed Vibration Frequencies of CaNCO, CaNNN, and CaNCS (in cm^{-1})

	CaNCO		CaNNN		CaNCS
Mode	Calculated[a]	Experimental[b]	Calculated[a]	Experimental	Calculated[a]
ν_1 (σ) sym NXX str	2214	2200	2191	2114	2019
ν_2 (σ) antisym NXX str	1344		1327	1364	927
ν_3 (σ) Ca—N str	368	390	383	396	317
ν_4 (π) NXX bend	624		826		464
ν_5 (π) Ca—N—X bend	117		172	43	79

[a]Reference 97.
[b]Reference 94.
[c]Reference 96.

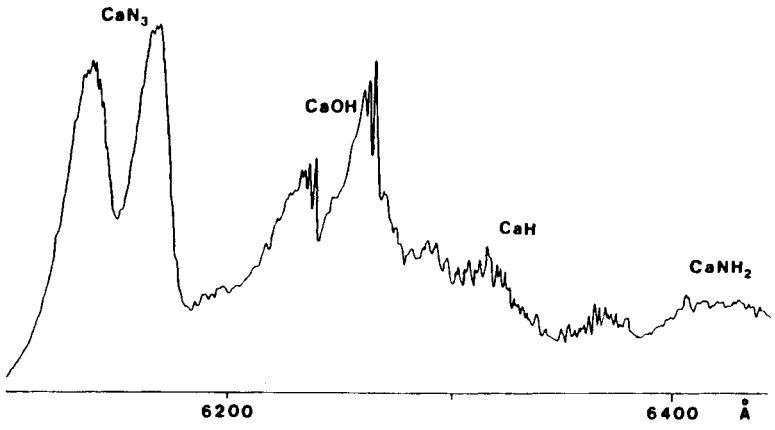

Figure 21. The chemiluminescence spectrum of the Ca + HN_3 reaction. [Reprinted with permission from ref. 96. Copyright 1988 American Institute of Physics.]

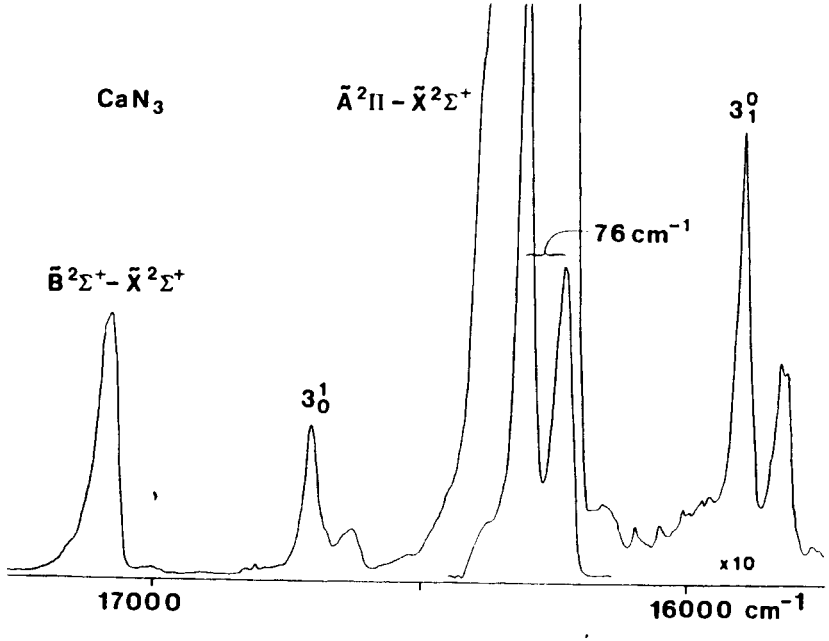

Figure 22. The dispersed fluorescence spectrum of CaN_3 [96]. The laser is exciting the 0–0 band of the $\tilde{A}^2\Pi_{3/2}$ - $\tilde{X}^2\Sigma^+$ transition of CaN_3. The $\tilde{A}^2\Pi$ state has a spin–orbit splitting of 76 cm^{-1}. [Reprinted with permission from ref. 96. Copyright 1988 American Institute of Physics.]

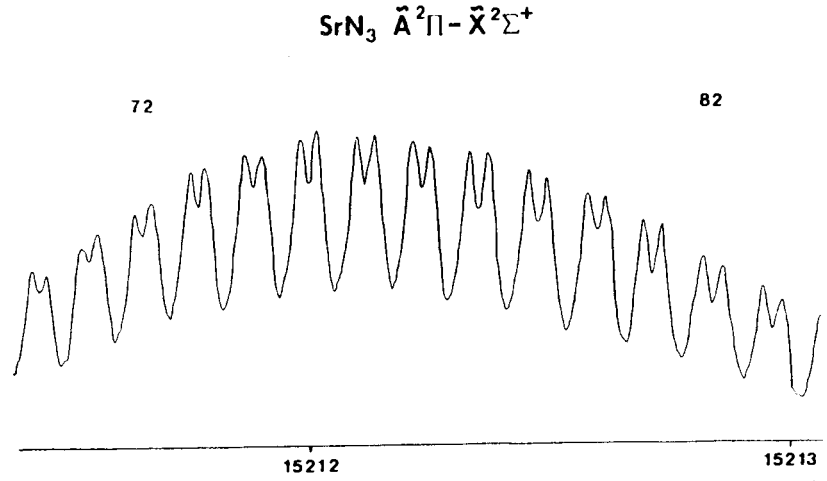

Figure 23. The high-resolution laser excitation spectrum of the $\tilde{A}^2\Pi_{3/2}$ - $\tilde{X}^2\Sigma^+$ transition of SrN_3 recorded using a monochromator as a narrow band filter. [Reprinted with permission from ref. 96. Copyright 1988 American Institute of Physics.]

by chemiluminescence (Fig. 21) and by low-resolution laser-induced fluorescence (Fig. 22). A rotational analysis of the $\tilde{A}^2\Pi$ - $\tilde{X}^2\Sigma^+$ transition (Fig. 23) of SrN_3 was carried out and confirmed the linear geometry [96].

The vibrational frequencies of CaN_3 were measured by fixing the laser on an electronic transition and dispersing the fluorescence with a small monochromator [96]. In this way, it was possible to measure four out of the five expected vibrational frequencies (Table 4). In general, the agreement with the ab initio predictions of Chan and Hamilton [97] is excellent except for the low-frequency metal–ligand bending mode. In this case, the interval of 86 cm^{-1} was measured by laser-induced fluorescence and interpreted as $2\nu_5$ since the selection rules forbid $\Delta v = \pm 1$ transitions for nontotally symmetric vibrational modes like ν_5. It would be expected that the ab initio calculations would have difficulty in predicting such a low frequency in an ionic molecule.

G. Monoisocyanides, MNC and Monocyanides, MCN

In many ways, the alkaline earth monoisocyanides have generated the most widespread interest and still remain the most mysterious of the molecules discussed in this chapter. The CaNC, SrNC, and BaNC molecules were

discovered by Pasternack and Dagdigian in 1976 [98] through chemiluminescent emission and low-resolution laser excitation spectra of the products of the reactions of Ca, Sr, and Ba vapors with BrCN. Additional chemiluminescent spectra of the Ca(^1D) reaction with BrCN were recorded by Furio and Dagdigian [99].

The problems (and the most interesting features) found in the spectroscopy of ionic metal cyanides and isocyanides occur because the CN^- ligand is nearly spherical. The CN^- ligand thus has a low barrier–internal rotation in M^+CN^- molecules. The equilibrium structure in the ground state can be linear cyanide, MCN, linear isocyanide, MNC, or even a *T*-shaped side-on complex (e.g., Na^+N^-). The molecular geometry is evidently determined by

a sensitive balance between competing factors that are not well understood. Clementi et al. [100] discuss this problem in 1973 and coined the term "polytopic bonding."

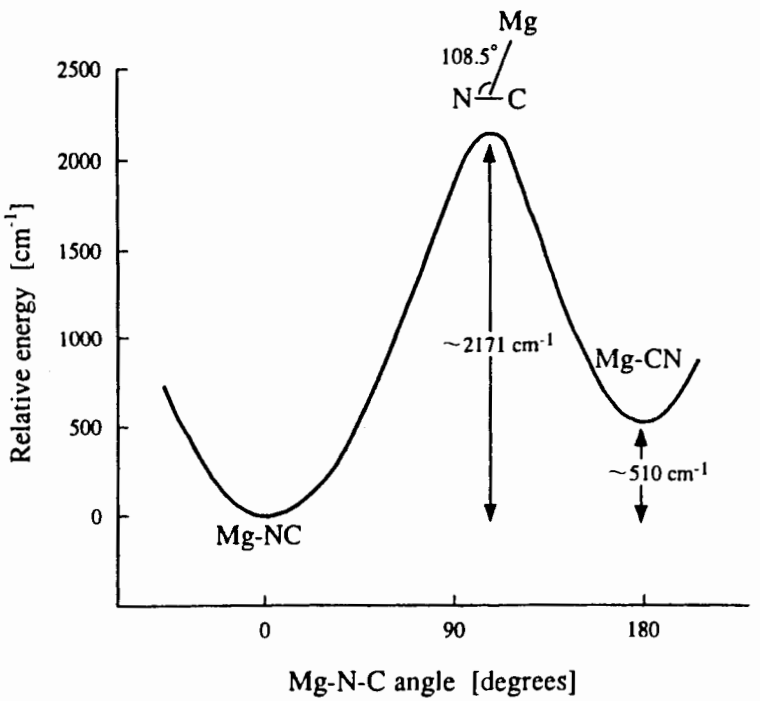

Figure 24. The bending potential surface of MgNC [107] as calculated by Ishii et al. [26]. [Reprinted with permission from ref. 107. Copyright 1996 American Institute of Physics.]

The problem of the molecular geometry of the alkaline earth cyanides was "solved" in 1985 when Bauschlicher et al. [101] calculated that the isocyanide structures, MNC, are the most stable (Fig. 24). They found that the BeNC and MgNC molecules have barriers between the isocyanide and cyanide linkage isomers (Fig. 24) but that the heavier metals, Ca, Sr, and Ba do not. More recent calculations on MgNC [26] support this general picture for the ground $\tilde{X}^2\Sigma^+$ states.

The excited states of CaNC and SrNC are not well understood although high-resolution spectra have been recorded in the ultracold environment of a molecular beam. The low-lying excited states of CaNC and SrNC should be $\tilde{A}^2\Pi$ and $\tilde{B}^2\Sigma^+$ analogous to CaF (Fig. 7). However, additional unassigned broad red emission is seen in both the Broida oven [102] and molecular beam experiments [39].

The Steimle group has extensively analyzed the $\tilde{A}^2\Pi$–$\tilde{X}^2\Sigma^+$ transition (Fig. 25) of normal CaNC [103] as well as the $Ca^{15}NC$ and $CaN^{13}C$ [104] isotopomers. They obtained a substitution structure with a CaN bond length of 2.207 Å and a CN bond length of 1.119 Å [104] in moderate agreement with the theoretical values [101] of 2.27 and 1.16 Å. A large dipole moment of 6.90 Å was found for the ground $\tilde{X}^2\Sigma^+$ state consistent with an ionic Ca^+NC^- structure [103]. The most interesting result, however, was the observation of large positive Λ-doubling constants in the $\tilde{A}^2\Pi$ states consistent with the $\tilde{B}^2\Sigma^+$ state lying about 1000 cm^{-1} below the $\tilde{A}^2\Pi$ state (cf. Fig. 7). The spectra show no clear trace of the $\tilde{B}^2\Sigma^+$ state and the $\tilde{A}^2\Pi$ state is perturbed by some unknown lower state. An interpretation for all of these facts is that the $\tilde{B}^2\Sigma^+$ state is, in fact, a low-lying $\tilde{A}'^2A_1$ state with a *T*-shaped (or even a linear cyanide, CaCN) geometry. In this case, the $\tilde{A}'^2A_1$–$\tilde{X}^2\Sigma^+$ bands would have poor Franck–Condon factors but could give rise to red emission. A careful exploration of the ab initio potential energy surfaces of CaNC should be able to solve this problem [143].

There was excitement in the radioastronomical community with the recent discovery of MgNC in the outer atmosphere of a carbon star, IRC + 10216 [25]. Very few metal-containing molecules are known in cool sources because metals like Mg tend to be condensed in the form of grains. Kawaguchi et al. [25] were able to record a laboratory microwave spectrum of MgNC and comparison with six unidentified radio lines confirmed the presence of MgNC in the dusty envelope of IRC + 10216. Theoretical calculations of Ishii et al. [26] lent support to this claim with predicted equilibrium MgN and NC bond lengths of 1.945 and 1.170 Å, respectively. The vibrational frequencies were predicted as $\nu_1(\sigma)$ 2188, $\nu_2(\pi)$ 83, and ν_3 (σ) 539 cm^{-1}. Later millimeter wave work by Anderson and Ziurys [105] on $^{25}MgNC$ and $^{26}MgNC$ gave an r_0 structure with bond lengths of 1.924 Å (MgN) and 1.170 Å (NC).

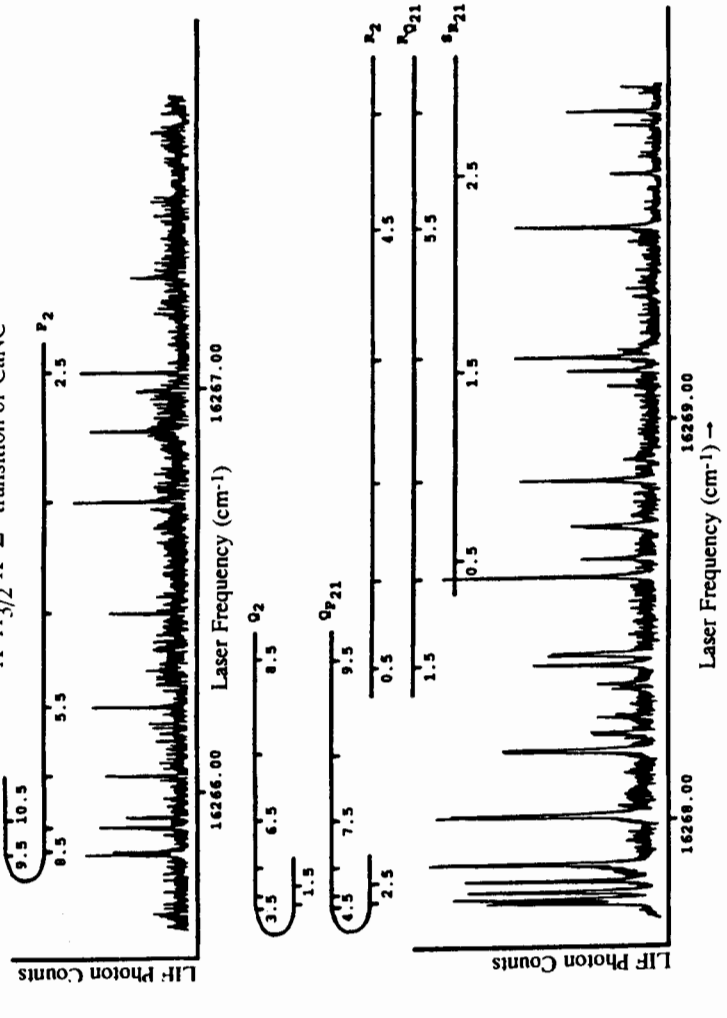

Figure 25. The high-resolution laser excitation spectrum of the $\tilde{A}^2\Pi_{3/2}-\tilde{X}^2\Sigma^+$ transition of jet-cooled CaNC. [Reprinted with permission from ref. 103. Copyright 1992 American Institute of Physics.]

The discovery of MgNC in the source IRC + 10216 sparked a great flurry of work on the rotational spectra of metal cyanides. Millimeter wave measurements were made for CaNC [106] and vibrationally excited states of MgNC [107]. In this later work, the ℓ-type doubling constant was used to estimate the bending frequency (ν_2) of 83 cm^{-1} for MgNC. The low-frequency microwave transitions of CaNC were measured in two molecular beam spectrometers in order to determine the hyperfine structure of the $\tilde{X}^2\Sigma^+$ state [108]. In all cases, the data could be interpreted in terms of a linear, ionic isocyanide structure. However, the low barrier–isomerization (Fig. 24) for MgNC or the lack of a barrier in the case of CaNC was evident in the anomalously large centrifugal distortion constants.

A barrier–isomerization of about 2000 cm^{-1} (Fig. 24) allows the metastable cyanide isomer, MgCN, to exist [26]. Anderson et al. [109] recorded the millimeter wave spectrum of the $\tilde{X}^2\Sigma^+$ state of MgCN along with very strong MgNC lines. These data allowed the identification of the MgCN isomer in the carbon star IRC + 10216 by radio astronomers [110].

H. Monohydrosulfides, MSH

The electronic spectra of CaSH and SrSH were first published in 1991 by Fernando et al. [111]. The molecules were made by the reaction of the electronically excited Ca* or Sr* atoms with H_2S. From the three electronic transitions $\tilde{A}^2A'-\tilde{X}^2A'$, $\tilde{B}^2A''-\tilde{X}^2A'$ and $\tilde{C}^2A'-\tilde{X}^2A'$ (Fig. 26) in the spectra, it was evident that CaSH and SrSH were bent molecules. Unlike the very ionic Ca^+OH^- molecule that prefers to keep the H(δ^+) atom as far as possible from Ca^+, the bonding in CaSH and SrSH is more covalent. The electronic spectra and orbitals in CaSH are very similar to the states of $CaNH_2$ but the lower symmetry (C_s) of CaSH changes the labels of the states ($\tilde{A}^2B_2$ to $\tilde{A}^2A'$, $\tilde{B}^2B_1$ to $\tilde{B}^2A''$ and $\tilde{C}^2A_1$ to $\tilde{C}^2A'$). The ab initio calculations of Ortiz [57] on CaSH confirm the bent geometry and this picture of the electronic structure.

Jarman and Bernath [112] carried out a rotational analysis of the $\tilde{A}^2A'-\tilde{X}^2A'$ transition (Fig. 26). The analysis yielded some fascinating results on the electronic structure in the $\tilde{A}^2A'$ state. Although CaSH is bent and the $A^2\Pi$ state of CaF has now been split into the $\tilde{A}^2A'$ and $\tilde{B}^2A''$ states (Fig. 7), the $\tilde{A}^2A'$ state is strongly affected by orbital angular momentum. Only molecules with a high symmetry such as linear ($C_{\infty v}$) can have orbital angular momentum and spin–orbit coupling. In particular, the large spin–orbit coupling constant ($A \sim 65\,\text{cm}^{-1}$) of the hypothetical linear CaSH molecule has been transformed to a large ε_{aa} spin–rotation constant (3.446 cm^{-1}) in the $\tilde{A}^2A'$ state. This large ε_{aa} constant in the $\tilde{A}^2A'$ state splits

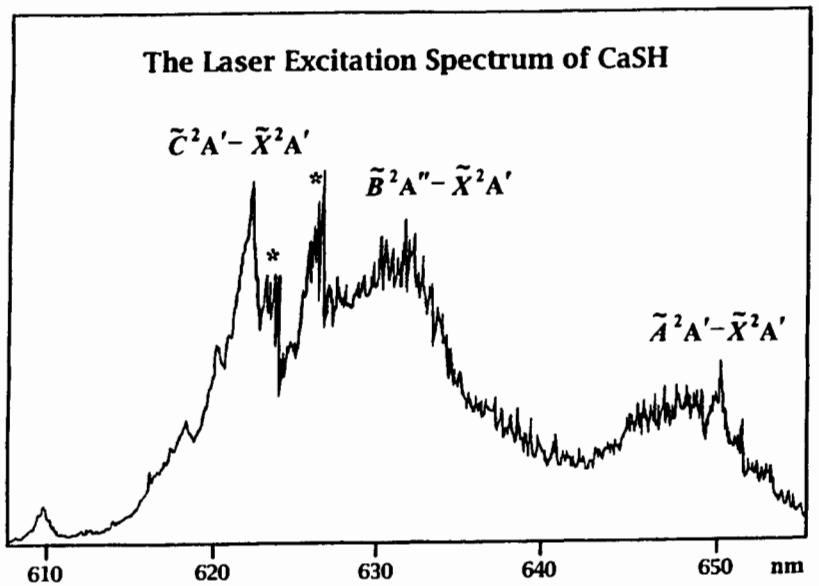

Figure 26. The laser excitation spectrum of the $\tilde{A}-\tilde{X}$, $\tilde{B}-\tilde{X}$, and $\tilde{C}-\tilde{X}$ transitions of CaSH [112]. The asterisks in this case mark CaOH impurity bands. [Reprinted with permission from ref. 112. Copyright 1993 American Institute of Physics.]

the two spin components linearly with increasing K_a (Fig. 27) so that only $K = 0$ obeys Hund's case (*b*) coupling and the higher K_a values obey Hund's case (a) coupling. K_a is the projection of the total angular momentum $\hat{\mathbf{N}}$ (exclusive of electron spin) onto the *a* inertial axis.

The $\tilde{B}^2A''-\tilde{X}^2A'$ electronic transition of CaSH was rotationally analyzed in a pulsed molecular beam source by Scurlock et al. [113]. The *a* axis of this asymmetric rotor lies very close to the Ca—S bond and there is a large dipole moment of 5.36 D projected along it in the $\tilde{X}^2A'$ state.

The millimeter wave spectra of CaSH, CaSD, and MgSH were recorded in Ottawa by Taleb-Bendiab et al. [114]. The pure rotational spectra of CaSH and CaSD allow an improved molecular geometry to be determined for the $\tilde{X}^2A'$ state. They found a r_0 Ca—S bond length of 2.564 Å, a S—H bond length of 1.357 Å, and a bond angle of 91°.

I. Monothiolates, MSR

The sulfur analogues of the alkaline earth monoalkoxides have also been made in a Broida oven by the reactions of Ca* and Sr* with thiols [111].

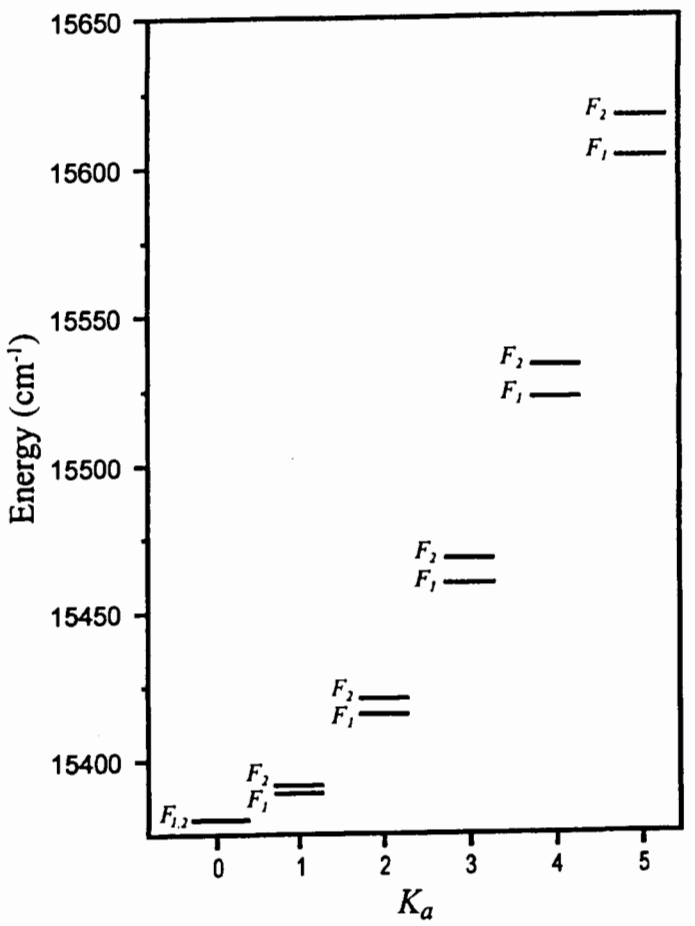

Figure 27. The spin splitting of the $\tilde{A}^2A'-\tilde{X}^2A'$ transition of CaSH as a function of K_a. The large value of ε_{aa} in the $\tilde{A}$ state causes the F_1 and F_2 components to split linearly with K_a. [Reprinted with permission from ref. 112. Copyright 1993 American Institute of Physics.]

The low-resolution laser excitation and fluorescence spectra of the $\tilde{A}-\tilde{X}$, $\tilde{B}-\tilde{X}$ and $\tilde{C}-X$ transitions of $CaSCH_3$, $SrSCH_3$, $CaSCH_2CH_3$, and so on, were recorded. The strong resemblance between the CaSH and CaSR spectra suggest that the monothiolates and monohydrosulfides have a similar electronic structure and that the Ca—S—C molecular backbone is bent.

J. Monoamides, MNH_2

The $CaNH_2$, $SrNH_2$, and $BaNH_2$ molecules were discovered by Wormsbecher et al. [32, 34] in Santa Barbara using a Broida oven. This work in the Harris group on amides and hydroxides was the crucial first step in the production of the now numerous monovalent derivatives of the alkaline earth metals. The electronic structure of $CaNH_2$ has already been discussed (Fig. 7) and Wormsbecher et al. [34] attempted a rotational analysis of the $\tilde{C}^2A_1-\tilde{X}^2A_1$ transition.

The $CaNH_2$ and $SrNH_2$ molecules, like CaSH, display three visible electronic transitions: $\tilde{C}^2A_1-\tilde{X}^2A_1$, $\tilde{B}^2B_1-\tilde{X}^2A_1$, and $\tilde{A}^2B_2-\tilde{X}^2A_1$ (Fig. 28). The $\tilde{A}-\tilde{X}$ and $\tilde{B}-\tilde{X}$ transitions of $SrNH_2$ are perpendicular transitions with K_a subband structure that spreads out while the $\tilde{C}-\tilde{X}$ transition has a transition dipole moment that lies along the Sr—N axis and K_a subbands that overlap (Fig. 28). A rotational analysis of the $\tilde{A}-\tilde{X}$ and $\tilde{B}-\tilde{X}$ transitions of $SrNH_2$ by Brazier and Bernath [115] confirmed the symmetries of the $\tilde{A}$ and $\tilde{B}$ states and they found an Sr—N bond length of 2.25 Å and an NH_2 bond angle of 104° in the $\tilde{X}$ state.

The molecular beam measurements of the $\tilde{A}^2B_2-\tilde{X}^2A_1$ and $\tilde{B}^2B_1-\tilde{X}^2A_1$ transitions of $CaNH_2$ by Whitham et al. [40] were pioneering experiments. Marr et al. [116] used the improved resolution of a CW dye laser to make a complete analysis of the $\tilde{A}-\tilde{X}$ transition. Like CaOH, $CaNH_2$ has a small dipole moment of 1.74 D in the ground $\tilde{X}^2A_1$ state. Marr et al. [116] also measured a large ε_{aa} spin-rotation constant in the $\tilde{A}^2B_2$ state.

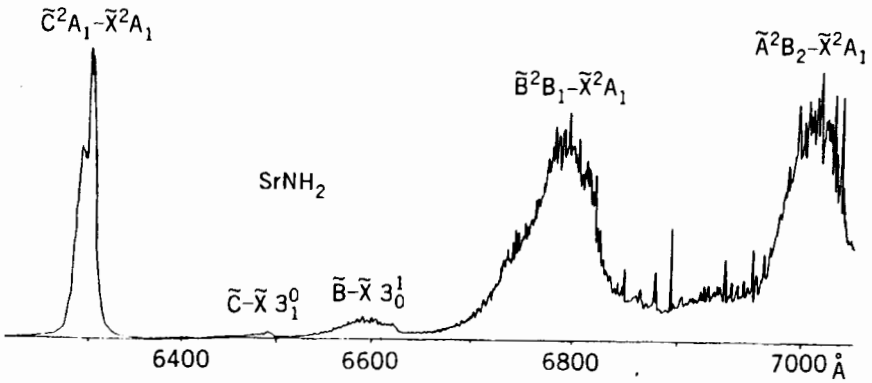

Figure 28. Laser excitation spectra of the $\tilde{A}-\tilde{X}$, $\tilde{B}-\tilde{X}$, and $\tilde{C}-\tilde{X}$ transitions of $SrNH_2$ [115].

TABLE 5 Experimental and ab initio Parameters for the $\tilde{X}^2A_1$ State of $CaNH_2$

	DFT[a]	Experimental[b]	
θ_{HNH}	105.6°	100.5°	102.9°
r_{NH} (Å)	1.02	1.041[c]	1.025[c]
r_{CaN} (Å)	2.13	2.118	2.140

Vibration		DFT (cm^{-1})[a]	Experimental ($\pm 10\,cm^{-1}$)[d]
ν_6 Antisym NH bend	b_2	345	320
ν_4 Out-of-plane bend	b_1	455	347
ν_3 Ca—N Stretch	a_1	544	520
ν_2 Sym NH bend	a_1	1586	
ν_1 Sym NH stretch	a_1	3448	
ν_5 Antisym NH stretch	b_2	3535	

[a]Density functional calculation (DFT), Reference 97.
[b]Reference 117.
[c]Fixed, see text.
[d]From low-resolution Broida oven experiments.

The $\tilde{B}^2B_1-\tilde{X}^2A_1$ and $\tilde{C}^2A_1-\tilde{X}^2A_1$ transitions have also been analyzed at Waterloo with a molecular beam spectrometer [117]. All three known electronic transitions have been fitted together to improve the molecular constants. The molecular geometry (Table 5) in the $\tilde{X}^2A_1$ state was found by fixing the N—H bond length to 1.041 Å (from NH_2^-) or 1.025 Å (from NH_2). Vibrational frequencies were measured by laser-induced fluorescence. For comparison (Table 5), Chan and Hamilton [97] calculated the molecular geometry and vibrational frequencies using density functional theory.

The most interesting aspect of the rotational analyses of the $\tilde{A}-\tilde{X}$, $\tilde{B}-\tilde{X}$ and $\tilde{C}-\tilde{X}$ transitions are the values for the complete set of nine spin-rotation parameters of the $\tilde{A}$, $\tilde{B}$, and $\tilde{C}$ states (ε_{aa}, ε_{bb}, and ε_{cc} for each state). If the orbitals containing the unpaired electron in these three states (Fig. 7) are approximate by a set of p orbitals (p_x, p_y, p_z) then all nine spin–rotation constants can be easily estimated by pure precession relationships.

Van Vleck introduced the pure precession approximation for diatomic molecules. The basic idea is that if the one-electron atomic orbital angular momentum is preserved in a diatomic molecule then the Λ-doubling and spin–rotation constants can be predicted, for example, in a $4p\sigma(^2\Sigma^+)$ and a $4p\pi(^2\Pi)$ state. This pure precession picture can easily be generalized to

TABLE 6 Spin-Rotation Parameters for the $\tilde{A}^2B_2$, $\tilde{B}^2B_1$, and $\tilde{C}^2A_1$ States of $CaNH_2$[a]

Parameter		$\tilde{A}^2B_2$	$\tilde{B}^2B_1$	$\tilde{C}^2A_1$
ε_{aa}	Observed	8.236	−7.547	0.998
	Pure precession	8.193	−8.193	0
	Formula[b]	$\frac{4AA^{SO}}{\Delta E_{B-A}}$	$\frac{4AA^{SO}}{\Delta E_{B-A}}$	0
ε_{bb}	Observed	0.00530	0.00351	−0.0398
	Pure precession	0	0.0539	−0.0547
	Formula	0	$\frac{4BA^{SO}}{\Delta E_{C-B}}$	$\frac{-4BA^{SO}}{\Delta E_{C-B}}$
ε_{cc}	Observed	0.0558	0.0381	−0.0385
	Pure precession	0.0418	0	−0.0417
	Formula	$\frac{4CA^{SO}}{\Delta E_{C-A}}$	0	$\frac{-4CA^{SO}}{\Delta E_{C-A}}$

[a]Reference 47.
[b]$A^{SO} = 66.80\,cm^{-1}$ spin–orbit constant of CaOH.

polyatomic molecules and used to predict the spin–rotation parameters ε_{aa}, ε_{bb}, and ε_{cc} of the interacting electronic states [117]. The results of this model are presented in Table 6. On the whole, the agreement is between experiment and prediction is reasonable with the greatest discrepancies occurring because of vibronic interactions in the $\tilde{B}$ state.

K. Monoalkylamides, MNHR

The preparation and low-resolution spectra of a few calcium and strontium alkylamides were reported in 1987 [118]. By replacing NH_3 with monoalkylamines, NH_2R [$R = -CH_3$, $-C_2H_5$, $-CH(CH_3)_2$, and $-C(CH_3)_3$] in a Broida oven, the laser-induced fluorescence spectra of the $\tilde{A}$–$\tilde{X}$, $\tilde{B}$–X, and $\tilde{C}$–$\tilde{X}$ transitions (see for example, Fig. 29) were recorded. There was a strong similarity with the spectra of $CaNH_2$ (Fig. 7) although the symmetry is lower than C_{2v} for the monoalkylamide derivatives.

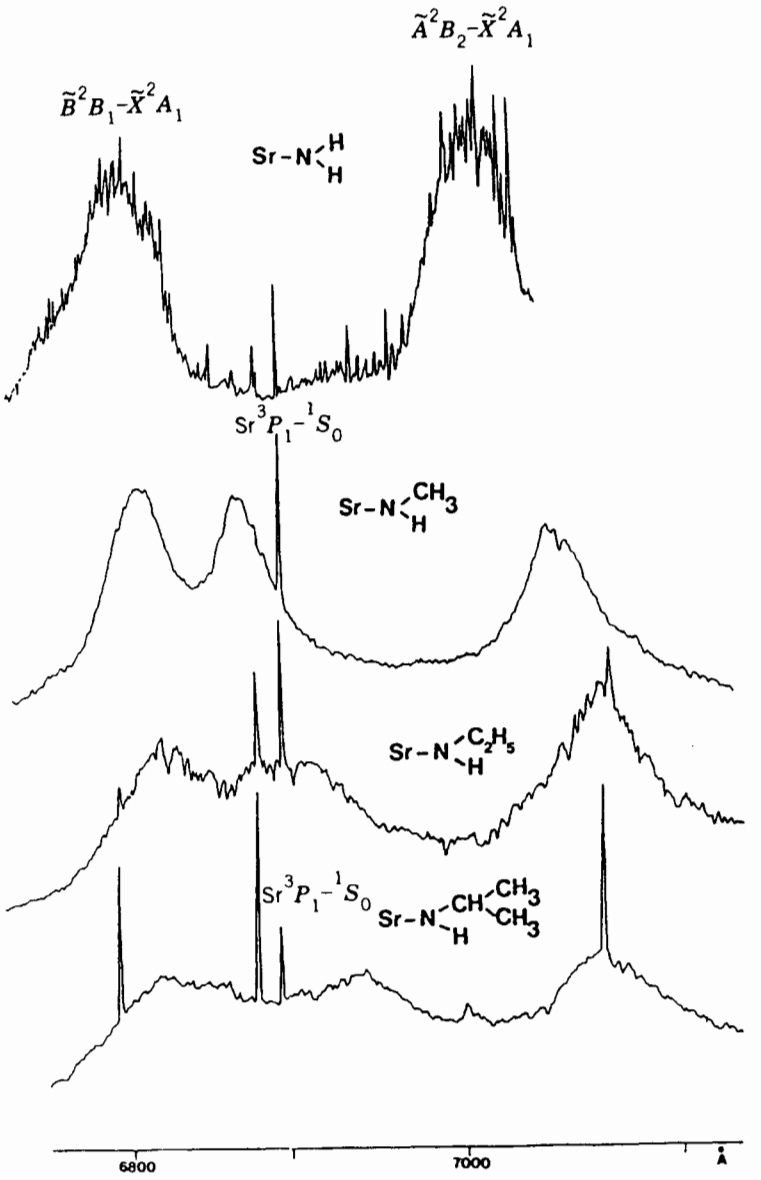

Figure 29. Laser excitation spectra of the $\tilde{A}$–$\tilde{X}$ and $\tilde{B}$–$\tilde{X}$ transitions of the strontium monoalkylamides. [Reprinted with permission from ref. 118. Copyright 1987 American Chemical Society.]

L. Monomethyls, MCH_3

The monomethyl derivatives are prototypical metal alkyl molecules, which can be made by the reactions of various methylating agents such as CH_3—N=N—CH_3, $Hg(CH_3)_2$, $Sn(CH_3)_4$, and CH_3CN with excited Mg, Ca, or Sr atoms. The low-resolution spectra of the $\tilde{A}^2E$–$\tilde{X}^2A_1$ and $\tilde{B}^2A_1$–$\tilde{X}^2A_1$ transitions of $CaCH_3$ and $SrCH_3$ were published by Brazier and Bernath [119] in 1987. These molecules have C_{3v} symmetry so that the electronic structure is similar to CaF (Fig. 7) but because of the reduction in symmetry the states are renamed ($^2\Pi \rightarrow {}^2E$, $^2\Sigma^+ \rightarrow {}^2A_1$). In this early work, upper limits for the metal–ligand dissociation energies of 46 and 43 kcal mol^{-1} for $CaCH_3$ and $SrCH_3$, respectively, were estimated from the onset of predissociation [119].

In view of the relatively weak metal–methyl bond, a measurement of the bond length would be useful. The $\tilde{A}^2E$–$\tilde{X}^2A_1$ transition of $CaCH_3$ was rotationally analyzed and the ground-state r_0 Ca—C bond length of 2.349 Å and H—C—H angle of 105.6° (with r_{C-H} fixed to 1.100 Å) were extracted [120]. The calculations of Ortiz [54] give $r_{Ca-C} = 2.388$ Å, $\theta_{HCH} = 105.9°$, and $r_{C-H} = 1.101$ Å. In Table 7, the experimental and predicted ground-state vibrational frequencies of $CaCH_3$ are compared. Tyerman et al. [112] calculated the ground-state properties of MCH, MCH_2, and MCH_3 for the lighter alkali and alkaline earth metals. The Arizona State University group recorded the millimeter wave spectra of $MgCH_3$ [122], $CaCH_3$ [123], $SrCH_3$ [124], and $BaCH_3$.

The $MgCH_3$ $\tilde{A}^2E$–$\tilde{X}^2A_1$ spectrum was analyzed in a laser ablation molecular beam spectrometer [125]. It was noted in this article that the ε_{aa} spin–rotation parameter in the $\tilde{A}$ state for $CaCH_3$ [120] seemed to have an anomalous sign when compared to the values obtained for $MgCH_3$, $ZnCH_3$, and $CdCH_3$. In fact, the original assignment of the excited state K values by Brazier and Bernath [120] was not correct because they did not see the first rotational lines of the branches. A reassignment of the $\tilde{A}^2E$–$\tilde{X}^2A_1$ transition of $CaCH_3$ by Marr et al. [126] using data from a molecular beam spectrometer corrected this problem and yielded a dipole moment of 2.62 D in the ground state. The power of the molecular beam method is illustrated clearly by this example.

TABLE 7 Experimental and Calculated Frequencies of $CaCH_3$ (in cm^{-1})

Mode	Observed Value[a]	Calculated Value[b]	Calculated Value[c]
ν_1 (a_1) sym C—H str		3023	3020
ν_2 (a_1) sym C—H bend	1085	1203	1104
ν_3 (a_1) Ca—C str	419	425	411
ν_4 (e) antisym C—H str		3100	3109
ν_5 (e) antisym H—C—H bend		1483	1443
ν_6 (e) Ca—C—H bend	318	385	356

[a]Reference 119.
[b]Reference 97.
[c]Reference 121.

M. Monoacetylides, MCCH

The monoacetylide derivatives are also important examples of simple organometallic molecules. The reactions of excited Ca and Sr with acetylene in a Broida oven resulted in the detection of the CaCCH and SrCCH molecules [127]. Table 8 compares the observed and calculated $\tilde{X}^2\Sigma^+$ vibrational frequencies. This work was rapidly followed by a rotational analysis of a vibrational band in the $\tilde{A}^2\Pi$–$\tilde{X}^2\Sigma^+$ transition of CaCCH [128]. It was assumed that we had found the 0–0 band, but the low-resolution molecular beam experiment of Whitham et al. [39] showed that we had analyzed a hot band.

Recently, several bands of the $\tilde{A}^2\Pi$–$\tilde{X}^2\Sigma^+$ transition of CaCCH were analyzed, first in a molecular beam source [129] and then in a Broida oven [130]. The pure rotational spectra of MgCCH [131], CaCCH [132], and SrCCH [133] are also available. If the C—H and C≡C bond lengths are fixed to 1.506 and 1.204 Å, then the Ca—C bond length is 2.349 Å, identical to the $CaCH_3$ value [132]. An ab initio calculation by Chan and Hamilton

TABLE 8 Ground-State Vibrational Frequencies of the CaCCH Molecule (in cm^{-1})

Mode	Experimental[a]	Calculated[b]
ν_1 (σ) C—H str		3507
ν_2 (σ) C≡C str		2466
ν_3 (σ) Ca—C str	399	383
ν_4 (π) C—C—H bend		701
ν_5 (π) Ca—C—C bend	90	197

[a]Reference 127.
[b]Reference 97.

[97] gives $r(CH) = 1.071$ Å, $r(C{\equiv}C) = 1.240$ Å and $r(Ca{-}C) = 2.368$ Å. Ab initio calculations are also available for MgCCH, $MgCCH^+$, $MgCH_3$ and MgC_2 [134]. The dipole moment of CaCCH (3.01 D) is also close to the value for $CaCH_3$ (2.62 D) in agreement with simple electrostatic models [129]. The laser excitation spectrum of the $\tilde{A}^2\Pi - \tilde{X}^2\Sigma^+$ transition of MgCCH has also been recorded [135]. Curiously, the spectra of CaCCH and SrCCH were originally recorded in an attempt to make the carbides CaC_2 and SrC_2 [127], and these species have still eluded detection.

N. Monocyclopentadienides, MC_5H_5

The sandwich complexes are among the most celebrated molecules in organometallic chemistry. The discovery of the structure of the ferrocene molecule, $Fe(C_5H_5)_2$, by Wilkinson was rewarded with a Nobel prize. The possibility of making half-sandwich complexes in the gas phase was very enticing and, inspired by a report of a metal vapor synthesis of magnesocene, $Mg(C_5H_5)_2$, we looked for CaC_5H_5 and SrC_5H_5 in a Broida oven [136]. The reaction of laser excited metal atoms with the cyclopentadiene precursor C_5H_6 resulted in the low-resolution spectra of the $\tilde{A}^2E_1 - X^2A_1$, and $\tilde{B}^2A_1 - \tilde{X}^2A_1$ transitions of CaC_5H_5 and SrC_5H_5.

The half-sandwich complexes have C_{5v} symmetry and the states are labeled in a similar way as for the metal monomethyls of C_{3v} symmetry. The spectra recorded by the Miller group [137, 138] for jet-cooled CaC_5H_5 allow a much improved vibrational analysis. Ultimately, in a spectroscopic tour-de-force, the $\tilde{A}^2E_1 - \tilde{X}^2A_1$ transition of CaC_5H_5 (Fig. 30) was rotationally analyzed and the Ca–ring distance of 2.333 Å was determined [139]. This metal–ring distance is very close to the Ca—C bond distance in the $CaCH_3$ and CaCCH molecules.

O. Monomethylcyclopentadienides, $MC_5H_4CH_3$

The first detection of a derivative of the monomethylsubstituted ligand $C_5H_4CH_3$ was carried out by Robles et al. [138] at Ohio State University. The substitution of a methyl group for an H atom on the ring lowers the symmetry to C_s from C_{5v} and lifts the double degeneracy in the $\tilde{A}^2E$ state (cf. Fig. 7). The A' and A'' components that correlate to the ^2E state of CaC_5H_5 are split by 100 cm^{-1}. The torsional splittings of the CH_3 group were also analyzed in the molecular beam experiment.

Figure 30. The high-resolution laser excitation spectrum of the 0_0^0 band of the $\tilde{A}^2E_{1(1/2)} - \tilde{X}^2A_1$ transition of CaC_5H_5. A simulation of the $K = 1-0$ subband is provided in the lower panel. [Reprinted with permission from ref. 139. Copyright 1995 American Institute of Physics.]

P. Monopyrrolates, MC_4H_4N

The isoelectronic analogy again proves to be very useful when the CH group of the $C_5H_5^-$ ligand is replaced by N to give the $C_4H_4N^-$ ligand. Laser excited Ca and Sr atoms reacted with the pyrrole C_4H_5N precursor in a Broida oven to give CaC_4H_4N and SrC_4H_4N [140]. The strong similarity between the monopyrrolates and the monocyclopentadienides led us to conclude that CaC_4H_4N and SrC_4H_4N were both half-sandwich complexes.

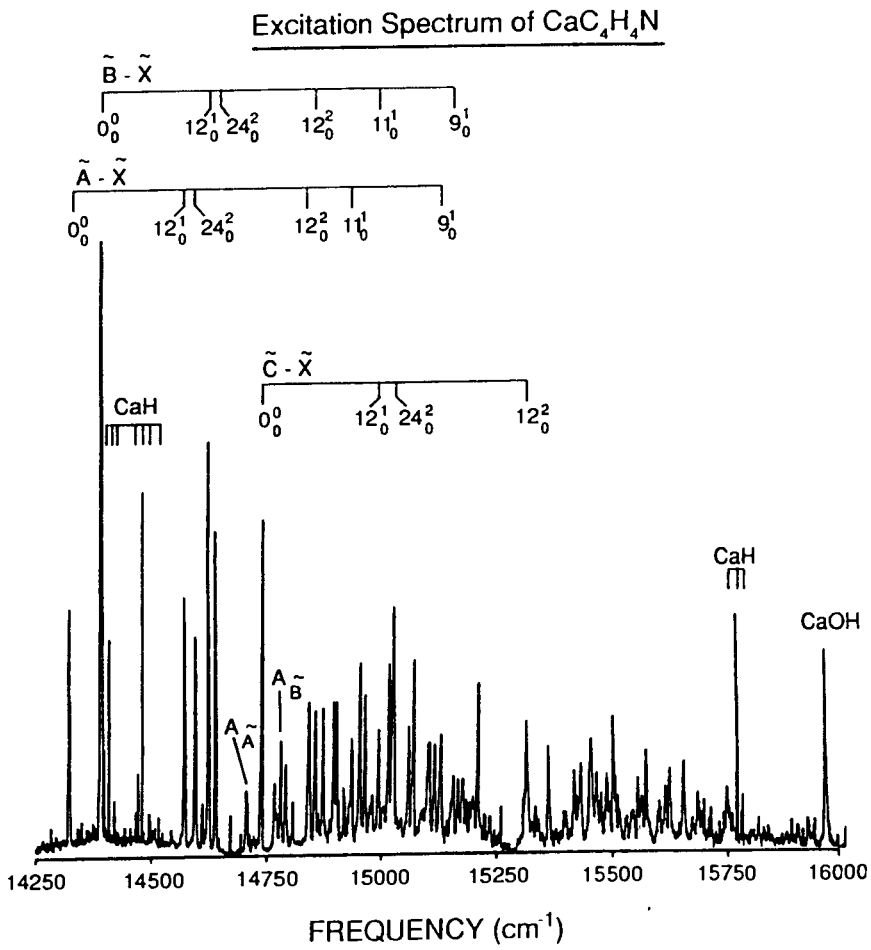

Figure 31. The laser excitation spectrum of the $\tilde{A}-\tilde{X}$, $\tilde{B}-\tilde{X}$, and $\tilde{C}-\tilde{X}$ transitions of jet-cooled CaC_4H_4N. [Reprinted with permission from ref. 138. Copyright 1992 American Chemical Society.]

Although this geometric structure turned out to be correct, there were problems with interpretation of the electronic structure in this early work.

Once again, it was jet cooling of CaC_4H_4N that clarified the problem [138]. The higher resolution spectra recorded in the Miller group did show that the ligand had η^5 coordination but that the lower C_s symmetry of CaC_4H_4N split the degenerate $\tilde{A}^2E$ state of CaC_5H_5 into two states. The 68-cm^{-1} splitting (Fig. 31) between these two electronic states of CaC_4H_4N was accidentally close to the expected spin–orbit splitting in a ^2E state and caused the confusion in the early work. A thorough vibrational analysis, made possible by the sharp bands in the cold spectrum, proved that the observed 68 cm^{-1} splitting was not a spin–orbit interval in the CaC_4H_4N molecule.

The MgC_5H_5, $MgC_5H_4CH_3$, and MgC_4H_4N molecules have also been synthesized in a pulsed jet source and their spectra analyzed [141]. The $\tilde{A}^2E_1$ state in MgC_5H_5 is very peculiar since it has no observable spin–orbit splitting. Unlike the metal-centered $\tilde{A}^2E$ states of the other molecules (e.g., CaC_5H_5 [56]) in MgC_5H_5, the unpaired electron is located on the C_5H_5 ring. In this case, the $\tilde{A}^2E_1-\tilde{X}^2A_1$ is a transition metal-to-ligand charge-transfer transition.

Q. Monoborohydrides, MBH_4

The $CaBH_4$ molecule completes the isoelectronic CaF, CaOH, $CaNH_2$, and $CaCH_3$ series of molecules. The Ca and Sr vapors react spontaneously with

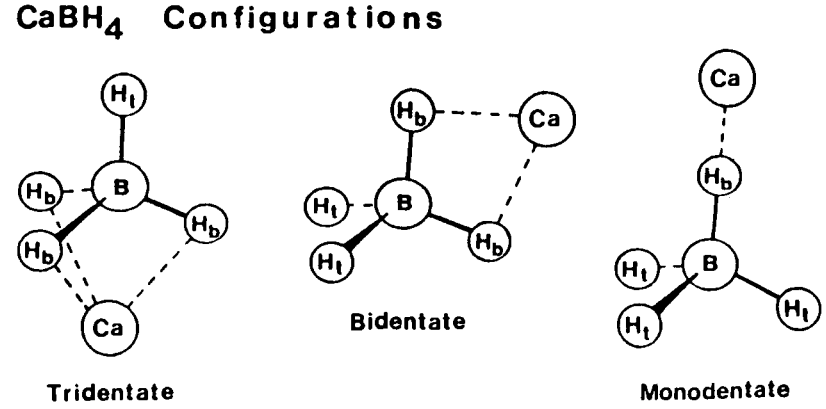

Figure 32. Three possible structures for the $CaBH_4$ molecule. The tridentate structure has the lowest energy. [Reprinted with permission from ref. 142. Copyright 1990 American Chemical Society.]

diborane, B_2H_6, to give $CaBH_4$ and $SrBH_4$. So far, there has been only one experimental paper written about these molecules [142]. The low-resolution laser-induced fluorescence spectra suggest that $CaBH_4$ and $SrBH_4$ have C_{3v} symmetry with the metal atom bonding to the face of the BH_4^- tetrahedron (Fig. 32). In addition, the ^2E and $^2A_1$ states seem to be switched compared to CaF (Fig. 7) so that one detects $\tilde{A}^2A_1-{}^2A_1$ and $\tilde{B}^2E-\tilde{X}^2A_1$ electronic transitions. The ab initio calculations of Ortiz [55] are in general agreement with our observations (although not in the ordering of the states) but more experimental work is necessary.

VI. CONCLUSIONS

The alkaline earth metals form a host of unique monovalent free radicals. Most of these molecules can be formed by the laser-driven chemical reactions of metal vapors with a wide variety of organic and inorganic molecules. This photochemical production of new molecules has led to an extensive gas-phase inorganic chemistry and spectroscopy of alkaline earth derivatives. In recent years, the Broida oven source has been displaced by the pulsed molecular beam spectrometer. The chemical dynamics and photochemistry of these new molecules are still at a very early stage of investigation.

ACKNOWLEDGMENTS

I thank my students and collaborators for their contributions to the work summarized here. At Arizona and Waterloo, this work was supported by NSF, Petroleum Research Fund, Office of Naval Research, Research Corporation, Natural Sciences and Engineering Research Council of Canada, and the Phillips Lab., Edwards AFB. I thank Z. Morbi, C. Zhao, F. Davis, T. Miller, T. Steimle and L. Zuirys for assistance with figures and for reprints and preprints. I also thank W. Chan and I. Hamilton for providing the results of their calculations in advance of publication.

REFERENCES

1. F. A. Cotton and G. Wilkinson, *Advanced Inorganic Chemistry*, 5th ed., Wiley-Interscience, New York, 1988.
2. D. E. Lessen, R. L. Asher, and P. J. Brucat, *J. Chem. Phys.* **93**, 6102 (1990).
3. K. F. Willey, C. S. Yeh, D. L. Robins, J. S. Pilgrim, and M. A. Duncan, *J. Chem. Phys.*, **97**, 8886 (1992).
4. C. T. Scurlock, S. H. Pullins, J. E. Reddic, and M. A. Duncan, *J. Chem. Phys.*, **104**, 4591 (1996).
5. M. H. Shen and J. M. Farrar, *J. Chem. Phys.*, **94**, 3322 (1991).
6. M. Sodupe and C. W. Bauschlicher, Jr., *Chem. Phys. Lett.*, **212**, 624 (1993).
7. C. W. Bauschlicher, Jr., M. Sodupe, and H. Partridge, *J. Chem. Phys.*, **96**, 4453 (1992).
8. T. P. Hanusa, *Chem. Rev.*, **93**, 1023 (1993).
9. E. Murad, *J. Chem. Phys.*, **75**, 4080 (1981).
10. C. W. Bauschlicher, Jr., S. R. Langhoff, and H. Partridge, *J. Chem. Phys.*, **84**, 901 (1986).
11. J. M. Brom, Jr., and W. Weltner, Jr., *J. Chem. Phys.*, **64**, 3894 (1976).
12. A. Antic-Jovanovic, V. Bojovic, and D. Pesic, *Spectrosc. Lett.*, **21**, 757 (1988); private communication with R. Colin.
13. J. Kong and R. J. Boyd, *J. Chem. Phys.*, **103**, 10070 (1995); **104**, 4055 (1996).
14. J. W. Kauffman, R. H. Hauge, and J. L. Margrave, *High Temp. Sci.*, **18**, 97 (1984).
15. J. F. W. Herschel, *Trans. R. Soc. Edinburgh*, **9**, 445 (1823).
16. R. F. Barrow and E. F. Caldin, *Proc. Phys. Soc. London Sect. B*, **62**, 32 (1949).
17. C. G. James and T. M. Sugden, *Nature (London)*, **175**, 333 (1955).
18. C. Th. J. Alkemade, Tj. Hollander, W. Snelleman, and P. J. Th. Zeegers, *Metal Vapours in Flames*, Pergamon, Oxford, UK, 1982.
19. E. Murad, W. Snider, and S. W. Benson, *Nature (London)*, **289**, 273 (1981).
20. T. Tsuji, *Astron. Astrophys.*, **23**, 411 (1973).
21. P. Pesch, *Astrophys. J.*, **174**, L155 (1972).
22. B. R. Pettersen and S. L. Hawley, *Astron. Astrophys.*, **217**, 187 (1989).
23. W. L. Barclay, Jr., M. A. Anderson, and L. M. Ziurys, *Chem. Phys. Lett.*, **196**, 225 (1992).
24. C. T. Scurlock, D. A. Fletcher, and T. C. Steimle, *J. Mol. Spectrosc.*, **159**, 350 (1993).
25. K. Kawaguchi, E. Kagi, T. Hirano, S. Takano, and S. Saito, *Astrophys. J.*, **406**, L39 (1993).
26. K. Ishii, T. Hirano, U. Nagashima, B. Weis, and K. Yamashita, *Astrophys. J.*, **410**, L43 (1993).
27. L. M. Ziurys, A. J. Apponi, M. Guélin, and J. Cernicharo, *Astrophys. J.*, **445**, L47 (1995).
28. P. F. Bernath, *Science*, **254**, 665 (1991).
29. S. J. Weeks, H. Haraguchi, and J. D. Winefordner, *J. Quant. Spectrosc. Radiat. Transfer*, **19**, 633 (1978).
30. P. A. Bonczyk, *Applied Opt.*, **28**, 1529 (1989).
31. P. A. Bonczyk, *Combust. Sci. Tech.*, **59**, 143 (1988).

32. R. F. Wormsbecher, M. Trkula, C. Martner, R. E. Penn, and D. O. Harris, *J. Mol. Spectrosc.*, **97**, 29 (1983).
33. J. Nakagawa, R. F. Wormsbecher, and D. O. Harris, *J. Mol. Spectrosc.*, **97**, 37 (1983).
34. R. F. Wormsbecher, R. E. Penn, and D. O. Harris, *J. Mol. Spectrosc.*, **97**, 65 (1983).
35. R. C. Hilborn, Q. Zhu, and D. O. Harris, *J. Mol. Spectrosc.*, **97**, 73 (1983).
36. J. B. West, R. S. Bradford, J. D. Eversole, and C. R. Jones, *Rev. Sci. Instrum.*, **46**, 164 (1975).
37. L. M. Ziurys, W. L. Barclay, Jr., M. A. Anderson, D. A. Fletcher, and J. W. Lamb, *Rev. Sci. Instrum.*, **65**, 1517 (1994).
38. P. F. Bernath, *Spectra of Atoms and Molecules*, Oxford, New York, 1995.
39. C. J. Whitham, B. Soep, J.-P. Visticot, and A. Keller, *J. Chem. Phys.*, **93**, 991 (1990).
40. C. J. Whitham and Ch. Jungen, *J. Chem. Phys.*, **93**, 1001 (1990).
41. C. R. Brazier, L. C. Ellingboe, S. Kinsey-Nielsen, and P. F. Bernath, *J. Am. Chem. Soc.*, **108**, 2126 (1986).
42. C. R. Brazier, P. F. Bernath, S. Kinsey-Nielsen, and L. C. Ellingboe, *J. Chem. Phys.*, **82**, 1043 (1985).
43. M. D. Oberlander and J. M. Parson, *J. Chem. Phys.*, **105**, 5806 (1996).
44. H. F. Davis, A. G. Suits, Y. T. Lee, C. Alcaraz, and J.-M. Mestdagh, *J. Chem. Phys.*, **98**, 9595 (1993).
45. P. de Pujo, O. Sublemontier, J.-P. Visticot, J. Berlande, J. Cuvellier, C. Alcaraz, T. Gustavsson, J.-M. Mesdagh, and P. Meynadier, *J. Chem. Phys.*, **99**, 2533 (1993).
46. C. Alcaraz, J.-M. Mestdagh, P. Meynadier, P. de Pujo, J.-P. Visticot, A. Binet, and J. Cuvellier, *Chem. Phys. Lett.*, **156**, 191 (1989).
47. T. Gustavsson, C. Alcaraz, J. Berlande, J. Cuvellier, J.-M Mestdagh, P. Meynadier, P. de Pujo, O. Sublemontier, and J.-P. Visticot, *J. Mol. Spectrosc.*, **145**, 210 (1991).
48. M. Oberlander, R. P. Kampf, and J. M. Parson, *Chem. Phys. Lett.*, **176**, 385 (1991).
49. B. S. Cheong and J. M. Parson, *J. Chem. Phys.*, **100**, 2637 (1994).
50. M. Esteban, M. Garay, J. M. Garcia-Tijero, E. Verdasco, and A. Gonzalez Urena, *Chem. Phys. Lett*, **230**, 525 (1994).
51. J. M. Mestdagh, J.-P. Visticot, and P. F. Bernath, *Chem. Phys. Lett.*, **237**, 568 (1995).
52. S. F. Rice, H. Martin, and R. W. Field, *J. Chem. Phys.*, **82**, 5023 (1985).
53. Z. Morbi, Ph.D. Thesis, University of Waterloo, 1997.
54. J. V. Ortiz, *J. Chem. Phys.*, **92**, 6728 (1990).

55. J. V. Ortiz, *J. Am. Chem. Soc.*, **113**, 1102 (1991).
56. J. V. Ortiz, *J. Am. Chem. Soc.*, **113**, 3593 (1991).
57. J. V. Ortiz, *Chem. Phys. Lett.*, **169**, 116 (1990).
58. L. M. Ziurys, D. A. Fletcher, M. A. Anderson, and W. L. Barclay, Jr., *Astrophys. J. Suppl.*, **102**, 425 (1996).
59. D. A. Fletcher, M. A. Anderson, W. L. Barclay, Jr., and L. M. Ziurys, *J. Chem. Phys.*, **102**, 4334 (1995).
60. P. R. Bunker, M. Kolbuszewski, P. Jensen, M. Brumm, M. A. Anderson, W. L. Barclay, Jr., L. M. Ziurys, Y. Ni, and D. O. Harris, *Chem. Phys. Lett.*, **239**, 217 (1995).
61. B. P. Nuccio, A. J. Apponi, and L. M. Ziurys, *J. Chem. Phys.*, **103**, 9193 (1995).
62. L. M. Ziurys, W. L. Barclay, Jr., and M. A. Anderson, *Astrophys. J.*, **384**, L63 (1992).
63. M. A. Anderson, W. L. Barclay, Jr., and L. M. Ziurys, *Chem. Phys. Lett.*, **196**, 166 (1992).
64. M. A. Anderson, M. D. Allen, W. L. Barclay, Jr., and L. M. Ziurys, *Chem. Phys. Lett.*, **205**, 415 (1993).
65. B. Fernandez, *Chem. Phys. Lett.*, **259**, 635 (1996).
66. Y. Ni, D. O. Harris, and T. Steimle, private communication.
67. R. Pereira and D. H. Levy, *J. Chem. Phys.*, **105**, 9733 (1996).
68. D. A. Fletcher, K. Y. Jung, C. T. Scurlock, and T. C. Steimle, *J. Chem. Phys.*, **98**, 1837 (1993).
69. T. C. Steimle, D. A. Fletcher, K. Y. Jung, and C. T. Scurlock, *J. Chem. Phys.*, **96**, 2556 (1992).
70. C. W. Bauschlicher, Jr., S. R. Langhoff, T. C. Steimle, and J. E. Shirley, *J. Chem. Phys.*, **93**, 4179 (1990).
71. J. M. Mestdagh and J. P. Visticot, *Chem. Phys.*, **155**, 79 (1991).
72. A. R. Allouche and M. Aubert-Frécon, *J. Mol. Spectrosc.*, **163**, 599 (1994).
73. R. A. Hailey, C. N. Jarman, W. T. M. L. Fernando, and P. F. Bernath, *J. Mol. Spectrosc.*, **147**, 40 (1991).
74. C. Zhao, P. G. Hajigeorgiou, P. F. Bernath, and J. W. Hepburn, *J. Mol. Spectrosc.*, **176**, 268 (1996).
75. P. I. Presunka and J. A. Coxon, *Chem. Phys.*, **190**, 97 (1995).
76. P. I. Presunka and J. A. Coxon, *J. Chem. Phys.*, **101**, 201 (1994).
77. P. I. Presunka and J. A. Coxon, *Can. J. Chem.*, **71**, 1689 (1993).
78. J. A. Coxon, M. Li, and P. I. Presunka, *J. Mol. Spectrosc.*, **150**, 33 (1991).
79. M. Li and J. A. Coxon, *Can. J. Phys.*, **72**, 1200 (1994).
80. J. A. Coxon, M. Li, and J. A. Coxon, *J. Mol. Spectrosc.*, **164**, 118 (1994).
81. J. A. Coxon, M. Li, and P. I. Presunka, *Mol. Phys.*, **76**, 1463 (1992).
82. M. Li and J. A. Coxon, *J. Chem. Phys.*, **97**, 8961 (1992).

83. M. Li and J. A. Coxon, *J. Chem. Phys.*, **102**, 2663 (1995).
84. M. Li and J. A. Coxon, *J. Chem. Phys.*, **104**, 4961 (1996).
85. C. N. Jarman and P. F. Bernath, *J. Chem. Phys.*, **97**, 1711 (1992); see also Z. J. Jakubek and R. W. Field, *J. Chem. Phys.*, **98**, 6574 (1993).
86. W. T. M. L. Fernando, M. Douay, and P. F. Bernath, *J. Mol. Spectrosc.*, **144**, 344 (1990).
87. R. Hailey, C. Jarman, and P. F. Bernath, *J. Chem. Phys.* (in press). R. Hailey, M.Sc. Thesis, University of Arizona, Tucson, 1991.
88. R. F. Wormsbecher and R. D. Suenram, *J. Mol. Spectrosc.*, **95**, 391 (1982).
89. L. C. O'Brien, C. R. Brazier, and P. F. Bernath, *J. Mol. Spectrosc.*, **130**, 33 (1988).
90. J. Brown, and T. Steimle private communication.
91. C. Zhao and P. F. Bernath, work in progress.
92. L. C. O'Brien, C. R. Brazier, S. Kinsey-Nielsen, and P. F. Bernath, *J. Phys. Chem.*, **94**, 3543 (1990).
93. A. M. R. P. Bopegedera, W. T. M. L. Fernando, and P. F. Bernath, *J. Phys. Chem.*, **94**, 3547 (1990).
94. L. C. Ellingboe, A. M. R. P. Bopegedera, C. R. Brazier, and P. F. Bernath, *Chem. Phys. Lett.*, **126**, 285 (1986).
95. L. C. O'Brien and P. F. Bernath, *J. Chem. Phys.*, **88**, 2117 (1988).
96. C. R. Brazier and P. F. Bernath, *J. Chem. Phys.*, **88**, 2112 (1988).
97. W.-T. Chan and I. P. Hamilton, private communication.
98. L. Pasternack and P. J. Dagdigian, *J. Chem. Phys.*, **65**, 1320 (1976).
99. N. Furio and P. J. Dagdigian, *Chem. Phys. Lett.*, **115**, 358 (1985).
100. E. Clementi, H. Kistenmacher, and H. Popkie, *J. Chem. Phys.*, **58**, 2460 (1973).
101. C. W. Bauschlicher, Jr., S. R. Langhoff, and H. Partridge, *Chem. Phys. Lett.*, **115**, 124 (1985).
102. M. Douay and P. F. Bernath, *Chem. Phys. Lett.*, **174**, 230 (1990).
103. T. C. Steimle, D. A. Fletcher, K. Y. Jung, and C. T. Scurlock, *J. Chem. Phys.*, **97**, 2909 (1992).
104. C. T. Scurlock, D. A. Fletcher, and T. C. Steimle, *J. Chem. Phys.*, **101**, 7255 (1994).
105. M. A. Anderson and L. M. Ziurys, *Chem. Phys. Lett.*, **231**, 164 (1994); also, M. Guélin, M. Forestini, L. M. Ziurys, M. A. Anderson, J. Cernicharo, and C. Kalhane, *Astron. Astrophys.* **297**, 183 (1995).
106. T. C. Steimle, S. Saito, and S. Takano, *Astrophys. J.*, **410**, L49 (1993).
107. E. Kagi, K. Kawaguchi, S. Takano, and T. Hirano, *J. Chem. Phys.*, **104**, 1263 (1996).
108. C. T. Scurlock, T. C. Steimle, R. D. Suenram, and F. J. Lovas, *J. Chem. Phys.*, **100**, 3497 (1994).
109. M. A. Anderson, T. C. Steimle, and L. M. Ziurys, *Astrophys. J.*, **429**, L41 (1994).

110. L. M. Ziurys, A. J. Apponi, M. Guélin, and J. Cernicharo, *Astrophys. J.*, **445**, L47 (1995).
111. W. T. M. L. Fernando, R. S. Ram, L. C. O'Brien, and P. F. Bernath, *J. Phys. Chem.*, **95**, 2665 (1991).
112. C. N. Jarman and P. F. Bernath, *J. Chem. Phys.*, **98**, 6697 (1993).
113. C. T. Scurlock, T. Henderson, S. Bosely, K. Y. Jung, and T. C. Steimle, *J. Chem. Phys.*, **100**, 5481 (1994).
114. A. Taleb-Bendiab, F. Scappini, T. Amano, and J. K. G. Watson, *J. Chem. Phys.*, **104**, 7431 (1996).
115. C. Brazier and P. F. Bernath, in preparation.
116. A. J. Marr, M. Tanimoto, D. Goodridge, and T. C. Steimle, *J. Chem. Phys.*, **103**, 4466 (1995).
117. Z. Morbi, C. Zhao, and P. F. Bernath, *J. Chem. Phys.*, **106**, 4860 (1997).
118. A. M. R. P. Bopegedera, C. R. Brazier, and P. F. Bernath, *J. Phys. Chem.*, **91**, 2779 (1987).
119. C. R. Brazier and P. F. Bernath, *J. Chem. Phys.*, **86**, 5918 (1987).
120. C. R. Brazier and P. F. Bernath, *J. Chem. Phys.*, **91**, 4548 (1989).
121. S. C. Tyerman, G. K. Corlett, A. M. Ellis, and T. A. Claxton, *Theochem.*, **364**, 107 (1996).
122. M. A. Anderson and L. M. Ziurys, *Astrophys. J.*, **452**, L157 (1995).
123. M. A. Anderson and L. M. Ziurys, *Astrophys. J.*, **460**, L77 (1996).
124. M. A. Anderson, J. S. Robinson, and L. M. Ziurys, *Chem. Phys. Lett.*, **257**, 471 (1996).
125. R. Rubino, J. M. Williamson, and T. A. Miller, *J. Chem. Phys.*, **103**, 5964 (1995).
126. A. J. Marr, F. Grieman, and T. C. Steimle, *J. Chem. Phys.*, **105**, 3930 (1996).
127. A. M. R. P. Bopegedera, C. R. Brazier, and P. F. Bernath, *Chem. Phys. Lett.*, **136**, 97 (1987).
128. A. M. R. P. Bopegedera, C. R. Brazier, and P. F. Bernath, *J. Mol. Spectrosc.*, **129**, 268 (1988).
129. A. J. Marr, J. Perry, and T. C. Steimle, *J. Chem. Phys.*, **103**, 3861 (1995).
130. M. Li and J. A. Coxon, *J. Mol. Spectrosc.*, **176**, 206 (1996); **180**, 287 (1996); **183**, 250 (1987).
131. M. A. Anderson and L. M. Ziurys, *Astrophys. J.*, **439**, L25 (1995).
132. M. A. Anderson and L. M. Ziurys, *Astrophys. J.*, **444**, L57 (1995).
133. B. P. Nuccio, A. J. Apponi, and L. M. Ziurys, *Chem. Phys. Lett.*, **247**, 283 (1995).
134. D. E. Woon, *Astrophys. J.*, **456**, 602 (1996); *J. Chem. Phys.*, **104**, 9495 (1996).
135. G. K. Corlett, A. M. Little, and A. M. Ellis, *Chem. Phys. Lett.*, **249**, 53 (1996).
136. L. C. O'Brien and P. F. Bernath, *J. Am. Chem. Soc.*, **108**, 5017 (1986).
137. A. M. Ellis, E. S. J. Robles, and T. A. Miller, *J. Chem. Phys.*, **94**, 1752 (1991).

138. E. S. J. Robles, A. M. Ellis, and T. A. Miller, *J. Am. Chem. Soc.*, **114**, 7171 (1992).

139. T. M. Cerny, J. M. Williamson, and T. A. Miller, *J. Chem. Phys.*, **102**, 2372 (1995).

140. A. M. R. P. Bopegedera, W. T. M. L. Fernando, and P. F. Bernath, *J. Phys. Chem.*, **94**, 4476 (1990).

141. E. S. J. Robles, A. M. Ellis, and T. A. Miller, *J. Phys. Chem.*, **96**, 8791 (1992).

142. F. S. Pianalto, A. M. R. P. Bopegedera, W. T. M. L. Fernando, R. Hailey, L. C. O'Brien, C. R. Brazier, P. C., Keller, and P. F. Bernath, *J. Am. Chem. Soc.*, **112**, 7900 (1990).

143. S. Nanbu, S. Minamino and M. Aoyagi, *J. Chem. Phys.* **106**, 8073 (1997).